Article:
Watson, CS, Carrivick, J and Quincey, D (2015) An improved method to represent DEM uncertainty in glacial lake outburst flood propagation using stochastic simulations. Journal of Hydrology, 529 (3). 1373 - 1389. ISSN 0022-1694

https://doi.org/10.1016/j.jhydrol.2015.08.046

An improved method to represent DEM uncertainty in glacial lake outburst flood propagation using stochastic simulations

Cameron S Watson[1], Jonathan Carrivick[1], Duncan Quincey[1]

School of Geography and water@leeds, University of Leeds, Leeds, LS2 9JT, UK

Correspondence to: C. S. Watson (gy09csw@leeds.ac.uk)

Abstract

Modelling glacial lake outburst floods (GLOFs) or 'jökulhlaups', necessarily involves the propagation of large and often stochastic uncertainties throughout the source to impact process chain. Since flood routing is primarily a function of underlying topography, communication of digital elevation model (DEM) uncertainty should accompany such modelling efforts. Here, a new stochastic first-pass assessment technique was evaluated against an existing GIS-based model and an existing 1D hydrodynamic model, using three DEMs with different spatial resolution. The analysis revealed the effect of DEM uncertainty and model choice on several flood parameters and on the prediction of socio-economic impacts. Our new model, which we call MC-LCP (Monte Carlo Least Cost Path) and which is distributed in the supplementary information, demonstrated enhanced 'stability' when compared to the two existing methods, and this 'stability' was independent of DEM choice. The MC-LCP model outputs an uncertainty continuum within its extent, from which relative socio-economic risk can be evaluated. In a comparison of all DEM and model combinations, the Shuttle Radar Topography Mission (SRTM) DEM exhibited fewer artefacts compared to those with the Advanced Spaceborne Thermal Emission and Reflection Radiometer Global Digital Elevation Model (ASTER GDEM), and were comparable to those with a finer resolution Advanced Land Observing Satellite Panchromatic Remote-sensing Instrument for

Stereo Mapping (ALOS PRISM) derived DEM. Overall, we contend that the variability we find between flood routing model results suggests that consideration of DEM uncertainty and pre-processing methods is important when assessing flow routing and when evaluating potential socio-economic implications of a GLOF event. Incorporation of a stochastic variable provides an illustration of uncertainty that is important when modelling and communicating assessments of an inherently complex process.

Keywords: GLOF, Flow path, Monte Carlo, Uncertainty, Digital Elevation Model, Bhutan

1. Introduction

Deglaciation is giving rise to a globally distributed increase in the number and size of glacial lakes (Carrivick and Tweed, 2013). In the Himalaya the trend of lake development is spatially variable in response to climate and the evolution of debris-covered glaciers (Gardelle et al., 2011; Benn et al., 2012; Nie et al., 2013). Sudden outbursts of large volumes of water from such lakes, termed Glacial Lake Outburst Floods (GLOFs) or 'jökulhlaups', can be hazardous to downstream communities and infrastructure. Hazardous lake identification is essential to direct timely remedial works, further investigations, or implement early warning strategies (Worni et al., 2012). The time to peak flow is usually short and lacks warning, meaning assessments of likely flood inundation become a primary tool for disaster preparedness (UNDMT, 2005; Koike and Takenaka, 2012; Takenaka et al., 2012). Application of a flood model can provide an indication of downstream exposure to a GLOF event, since flood propagation is primarily a function of the underlying topography and the GLOF hydrograph.

The shape and magnitude of the lake breach hydrograph determines the distribution and timing of the flood event, and is therefore a key component of a hazard assessment (Westoby et al., 2014). Complete GLOF hazard assessments follow a sequential source to impact methodology that usually comprises an investigation of lake dynamics, lake surroundings,

breach scenarios, and creating downstream risk assessments highlighting potential inundation zones (Worni et al., 2014). The current state of knowledge of the GLOF process chain was reviewed by Worni et al. (2014) and Westoby et al. (2014), who both highlighted that studies evaluating the propagation of uncertainty throughout the chain are lacking. Sources of uncertainty are discussed by Westoby et al. (2014) and Westoby et al. (2015). Briefly, they concern the initiating trigger mechanism, parameterisation of the dam-breach and initial dam conditions, and the hydrodynamic modelling itself. The hydrodynamic modelling has uncertainties arising from the topographic resolution used; channel roughness coefficients; model dimensionality; and model coupling between the trigger, breach, and flood. A probabilistic unified GLOF modelling workflow implemented by Westoby et al. (2015) addresses several sources of this cascading uncertainty, but has high data requirements. Such methods of addressing stochastic elements and compounding uncertainty should be implemented and communicated, concurrent with use of integrated workflows for assessing GLOF hazard (e.g. Huggel et al., 2002; Bolch et al., 2011; Mergili and Schneider, 2011; Worni et al., 2012; Mergili et al., 2013).

Where field data are insufficient to implement a physically based numerical flood model, or to guide their application, first-pass assessments are commonly implemented (e.g. Huggel et al., 2003; Mergili and Schneider, 2011; Mergili et al., 2013). These generally utilise medium resolution DEM products such as the ASTER GDEM (herein GDEM) and SRTM DEM (herein SRTM) which carry greater vertical uncertainty. Such coarser datasets can still be valuable for flood inundation modelling (e.g. Sanders, 2007). However, GIS-based algorithms using flow direction are highly sensitive to vertical errors in such DEMs (Veregin, 1997; Endreny and Wood, 2001). Additionally, a river channel is often poorly defined in coarse terrain data and may be offset compared to the ground truth channel and hence socio-economic infrastructure. This DEM error can be compounded by sink filling, which is a DEM

processing routine that can remove local elevation minima representing the channel (e.g. Czubski et al., 2013). Therefore communication of DEM uncertainty should accompany such first-pass modelling efforts since this uncertainty is intrinsically important for understanding flow propagation.

This paper therefore presents an inter-model comparison of two GIS-based first-pass flood assessment techniques and a 1D flood model. The Modified Single-Flow-direction (MSF) model developed by Huggel et al. (2003) was compared to the new MC-LCP developed herein, and also to a hydrodynamic model created using HEC-RAS. The aim of this study was to quantify the differences between methods when using the same underlying terrain data, and when using three different DEM products.

The first-pass MC-LCP GLOF assessment technique developed in this study incorporates the evaluation and communication of DEM uncertainty in the modelled output. It avoids the requirement of a flow direction grid and hence a 'filled' DEM. This increases its utility and minimises potential artefacts in low relief populated areas, for which a reliable inundation output is most desired. The method is proposed as an alternative first-pass GLOF vulnerability assessment for data poor regions and features a transferable, easily implemented, and adaptable methodology. It is applied to a case study in Bhutan to evaluate applicability in a high relief catchment using only remotely sensed data. Since this case study is purely hypothetical, the MC-LCP is also validated using geomorphic evidence of the 1985 Dig Tsho GLOF in Nepal.

2. Background

2.1 Previous assessment strategies

GLOF hazard assessments require consideration of the probability of an event occurring and the vulnerability of downstream communities and infrastructure, in order to make informed

decisions on the risk magnitude and hence suitable remediation or adaptation strategies. Studies may adopt a qualitative (e.g. Huggel et al., 2004a), semi-quantitative (e.g. Bolch et al., 2011), or quantitative approach (e.g. McKillop and Clague, 2007; Mergili and Schneider, 2011) using factor combinations of lake and dam characteristics, the surrounding lake topography, and adjacent glacier dynamics (Emmer and Vilímek, 2013). However, their combination and weighting in a hazard assessment is not standardised. Increasingly there is a transition towards modelling the source-to-impact GLOF process chain, using higher-order physically based models (Worni et al., 2014). However, constructing physically-based flood models is limited by the uncertainty and availability of remotely sensed parameters such as dam geometry (e.g. Worni et al., 2012), and the time investment in creating and applying such models. They nevertheless provide an enhanced understanding of GLOF flow characteristics where the paucity of high resolution terrain data limits most modelling efforts to using flow routing algorithms or 1D models, which cannot fully represent flow dynamics (Westoby et al., 2014).

Many previous studies have made use of medium-resolution DEM products such as ASTER-derived DEMs (e.g. Byers et al., 2013), and the GDEM and SRTM DEMs (e.g. Wang et al., 2012). These DEMs permit catchment-scale coverage where a similar extent of finer resolution products such as photogrammetry or airborne laser scanning would be otherwise limited logistically or prohibitively expensive. Additionally, the low data processing and storage requirements of the GDEM and SRTM permit their rapid exploitation and interrogation for simple flow models. However, these products contain inherent uncertainty in grid cell elevations of the same order in magnitude to a GLOF flow depth. This is most prevalent in mountainous terrain (Hayakawa et al., 2008; ASTER GDEM Validation Team, 2011; Kolecka and Kozak, 2014) since pixel resolution is less representative of terrain characteristics (Fisher and Tate, 2006). For the SRTM, elevation uncertainty contributes to a

systematic negative elevation bias with increasing altitude (Paul, 2008), identified in the French Alps (Berthier et al., 2006), and confirmed for the Himalaya (Berthier et al., 2007), though its precise origin is not apparent. For the GDEM, Rexer and Hirt (2014) demonstrated improved vertical accuracy compared to the SRTM over mountainous terrain in Australia. However, forested land cover contributed to a positive elevation bias for both the GDEM (ASTER GDEM Validation Team, 2011; Rexer and Hirt, 2014) and SRTM (Sun et al., 2003; Shortridge and Messina, 2011; Kolecka and Kozak, 2014).

Quantification of the potential implications of spatially variable elevations biases for GLOF modelling requires ground truth data, but nevertheless should be considered on a catchment by catchment basis. For example, GLOFs originate in high-altitude vegetation sparse environments and will generally flow through increasingly vegetated reaches, such that a general trend of increasingly positive elevation bias could exist with distance downstream in forested Himalayan reaches. Consideration of the uncertainty and spatial autocorrelation in medium resolution topographic products should therefore accompany their usage.

GIS-based assessments of GLOF routing and inundation provide a first-pass assessment tool to identify vulnerable catchments for further analysis (Huggel et al., 2004b), but may also be utilised to identify likely inundation characteristics at finer scales and hence an initial assessment of relative risk (Nussbaumer et al., 2014). The ArcGIS-based MSF model developed by Huggel et al. (2003) has seen usage for modelling GLOFs and debris flows (e.g. Huggel, 2004; Huggel et al., 2004b; Schneider et al., 2008; Frey et al., 2010; Iribarren Anacona et al., 2014; Nussbaumer et al., 2014). Similar procedures are available in GRASS GIS, weighting the flow propagation using local slope and flow direction (e.g. Mergili and Schneider, 2011; Gruber and Mergili, 2013). Hydrodynamic modelling is also feasible on global DEMs, though uncertainty is increased as a consequence of poorly resolved channel networks (e.g. Wang et al., 2012; Czubski et al., 2013).

Models dependent on the maintenance of flow direction require a hydrologically correct DEM with spurious sinks 'filled' to avoid the algorithm terminating. This filling raises pitted areas of the DEM surface and can lead to parallel flow artefacts where lengths of the channel are filled to similar elevations (Melles et al., 2011). Uncertainly introduced by filling is compounded by underlying DEM uncertainty; commonly reported as a root mean square error (RMSE). Therefore communication of the uncertainty in modelled flood extents would both increase the confidence in and utility of such first-pass assessments. An evaluation of DEM uncertainty can be gained by using stochastic simulation techniques such as the Monte Carlo method (Lindsay and Evans, 2008). In this study, a Monte Carlo approach allows modelled inundated areas to be evaluated based on their inundation frequency following an iterative process of flow routing over sequential terrain realisations, hence making predictions of socio-economic impacts more robust.

2.2 Bhutan case study

The Chamkhar Chu catchment in Bhutan was selected to exemplify a data-scarce site; hence requiring the use of globally available DEMs and a more simplistic inundation modelling approach. Here, the paucity of fine-resolution data sets, documented past events, or field surveys, limits the possible application of physically-based flood models. Simple GIS-based first-pass flood assessments such as the MSF or the MC-LCP proposed, therefore offer a fast and transferable alternative for delineating likely GLOF flow paths whilst also considering lateral extent.

Addressing GLOF risk became a priority in Bhutan following the 1994 GLOF event from Lugge Tsho (Watanbe and Rothacher, 1996; Ghimire, 2005). Remediation and early warning strategies were implemented through two internationally funded efforts involving the United Nations Development Program (UNDP) (Meenawat and Sovacool, 2011). Substinence

communities using mountain streams for agricultural irrigation are often located on elevated terraces away from the valley bottoms and hence flood risk (Wangdi and Kusters, 2012) but the long runout distance of GLOF peaks increases the vulnerability of downstream infrastructure and settlements located closer to the river channel (Takenaka et al., 2012). Safeguarding hydropower generation is of particular importance in Bhutan because it represents 99 % of electricity generation (Jamtsho, 2012), accounts for an estimated 22 % of Bhutan's GDP, and has secured investments in future run-of-the-river plants that are susceptible to runoff variability (NEC, 2009).

A study by Mool et al. (2001) identified the existence of 24 potentially dangerous glacial lakes in Bhutan (Figure 1); although a more recent GIS assessment considering dam slope suggests fewer exist (Fujita et al., 2013). Nevertheless, glacial lake expansion in Bhutan (Komori, 2008) and the expected enhanced glacial lake development on stagnant, debris-covered glaciers (Kääb, 2005), suggests the potential impact of future GLOFs should be continually evaluated.

[Figure 1 approximate location]

3. Data sources and pre-processing

3.1 DEMs

The ASTER GDEM V2. has ca. 30 m horizontal resolution and a reported vertical RMSE of ±15.1 m over mountainous terrain (ASTER GDEM Validation Team, 2011). The SRTM DEM 4.1 has 90 m horizontal resolution and a vertical RMSE of ca. ±16 m (Rexer and Hirt, 2014). Both are surface models, such that stated elevations reflect the tops of dense vegetation and built up areas. However, the SRTM sampling coincided with leaf-off conditions for northern hemisphere deciduous forests, suggesting that elevation data over forested regions may represent a mix signal between tree height and ground level elevations

(ASTER GDEM Validation Team, 2011). In the absence of finer resolution DEMs, both global datasets are used for hydrodynamic modelling (e.g. Gichamo et al., 2012; Wang et al., 2012). In this study, a third DEM was created at 15 m horizontal resolution using stereo ALOS PRISM scenes of 2.5 m resolution, and ground control points (GCPs) derived from Google Earth. The accuracy and resolution of the Google Earth elevation data is unknown, although good association has been demonstrated with ASTER and SRTM elevation data (e.g. Rusli et al., 2014). In this study, we assumed that the GCPs were of similar accuracy to the SRTM data and used a vertical RMSE of ±16 m for the ALOS DEM. Summary statistics showing the relative accuracy of each DEM are presented in Table 1, highlighting that our ALOS DEM is most comparable to the SRTM. The GDEM and SRTM were resampled to 15 m resolution using bilinear interpolation to provide a common pixel size for analysis in this study.

The spatial resolution of the GDEM and SRTM means that they cannot accurately represent a river valley with steep banks. Specifically, these DEMs contain spurious peaks and depressions that require pre-processing to improve flow routing (Fisher and Tate, 2006; Pitman et al., 2013). Since a DEM is modified by this pre-processing, several correction methods were considered in this study using the optimized pit removal tool (Soille, 2004; CRWR, 2013). All three DEMs were processed to minimise net change for the HEC-RAS and MC-LCP models. This was carried out automatically with the optimized pit removal tool which uses cut and fill operations to minimise DEM sinks. In this study, these are referred to as optimized pit removal net (OPRN) DEMs (Figure 2a). In contrast, we filled all three DEMs for use with the MSF model, which is a requirement for it to run and caused comparatively higher cell modification (Table 2). The mean difference between OPRN and 'filled' DEM profiles is smallest for the SRTM (5.6 m), followed by the ALOS (7.5 m) and GDEM (23.4 m) (Table 1), suggesting a higher incidence of channel artefacts in the GDEM.

[Figure 2 approximate location]

3.2 Socio-economic

Socio-economic impact was evaluated using a 2010 land cover dataset produced by Gilani et al., (2014), supplemented with a buildings and road network layer digitised from Google Earth imagery.

4. Methods

The MC-LCP model was evaluated against the MSF GIS-based model and a 1D hydrodynamic model using three DEM products of different initial resolutions, following the general workflow outlined in Figure 3.

[Figure 3 approximate location]

4.2 Monte Carlo Least Cost Path model (MC-LCP)

The MC-LCP model (Figure 4) was developed as part of this study and incorporates an iterative cost path analysis and Monte Carlo loop of modelled DEM uncertainty, and was implemented in ArcGIS 10.2. Similar to the MSF model, the MC-LCP has no physical basis and is proposed as a first-pass assessment technique. Incorporating stochastic DEM uncertainty within the model facilitates lateral spread and produces relative inundation probabilities for each DEM cell. Spatial autocorrelation of DEM error is a recognised quality issue, though is difficult to assess without a reference dataset and only a RMSE is commonly provided for global datasets (Carlisle, 2005; Wechsler, 2007). In this study, a spatial autocorrelation of RMSE uncertainty was introduced in each model iteration as six 15 m pixels for the GDEM, six 15 m pixels for the SRTM which is degraded from 30 m to 90 m horizontal resolution, and three 15 m pixels for the ALOS DEM, using a focal neighbourhood filter following Hebeler and Purves (2009) and Zandbergen (2011).

The MC-LCP model workflow is detailed in Figure 4, which describes the processes involved in the three aspects of the model: modelling DEM uncertainty, creating the cost layers, and modelling least cost path iterations. For each iteration, a normally distributed raster layer was created with a standard deviation matching the RMSE of each DEM and a mean of zero (Gatziolis and Fried, 2004; Zandbergen, 2011). Spatially autocorrelated uncertainty was then introduced with a neighbourhood filter. Each iteration of the error model was then added to the initial DEM, thereby creating a new terrain realisation (Lindsay and Evans, 2008). A cost path analysis was conducted between a start and end location defining the study reach, using equally weighted cost layers of vertical elevation difference from the river channel and local slope. This produced a pixel-wide downstream least cost path. Subsequent iterations producing new least cost paths were sequentially added, hence the final output represented the number of times each cell was considered a least cost path, and therefore inundated. In this study, outputs were initially evaluated at 50, 100, 500, 1000, and 1500 iterations for each DEM. Stable inundation extents were apparent at 500 model iterations (Figure 5), hence all subsequent least cost path results were derived using 500 iterations. The top one percent of inundated cells were excluded in this study to remove spurious paths. This exclusion is an arbitrary decision based on an inspection of the output where spurious paths diverge notably from the main distribution.

[Figure 4 approximate location]

[Figure 5 approximate location]

The MC-LCP model design produced a distribution of least cost paths down the study reach for which it is conceivable that a flood could inundate. The likelihood of inundation is represented by the inundation frequency output. In this study the lateral spread of least cost paths represents our first-pass assessment of GLOF extent. This is similar to a ‘random walk’ procedure implemented in GRASS GIS by Mergili and Schneider (2011) and Gruber and

Mergili (2013), which produced a lateral inundation extent weighted for local slope, but did not incorporate DEM uncertainty.

Applying a variable threshold to the inundation frequency output could be used to delineate a river network, since a high inundation frequency would be indicative of the valley bottom. Similar thresholding is used on the output of the flow accumulation function in ArcGIS to delineate a stream and river network, however this requires a 'filled' DEM (Melles et al., 2011). Where a ground truth river is unavailable, the model can be used to generate a least cost path down the study reach using the original DEM, i.e. no error model is applied. This would represent the input river channel (Figure 4) and can be derived from an OPRN processed DEM.

4.2.1 Dig Tsho validation

Although the MC-LCP output is not directly applicable to any particular magnitude of GLOF event, validation of the MC-LCP output was undertaken using geomorphic evidence of the 1985 Dig Tsho GLOF extent, which featured an estimated peak discharge of ca. 2000 $m^3 s^{-1}$ (Vuichard and Zimmermann, 1987). The six locations of GLOF geomorphic evidence mapped by Cenderelli and Wohl (2001) was used as the flood extent, which was compared to the MC-LCP modelled extent for the GDEM (Figure 6, Table 3). This validation used a least cost path derived river, therefore representing the MC-LCP in its simplest state without a ground truth river network.

Application of the MC-LCP to the 1985 Dig Tsho GLOF event revealed good spatial association with geomorphic evidence of the known GLOF extent (Figure 6, Table 3). Slight discrepancies between the 'flow path' of the MC-LCP and the field-measured extent were apparent in reach L1 and L8, which was attributed to the DEM resolution (30 m) misrepresenting the high relief channel, rather than potential contemporary river channel migration reflected in the DEM. However, overall the MC-LCP provided a good

representation of the 1985 GLOF extent with a mean classification accuracy of 78 % for the reaches mapped (Table 3).

[Figure 6 approximate location]

4.2.2 Additional land cover cost

Following the study of Nussbaumer et al. (2014), which considered multi-temporal GLOF risk following land use change, we modelled the influence of including an additional land cover cost factor into the MC-LCP, which we denote herein as MC-LCP LC; specifically on the inundated area and whether high-cost land covers such as woodland would consequently experience lower inundation. This was carried out using a simple reclassification of the land cover layer using Manning's N hydraulic roughness values following Chow (1959). When multiplied by 1000, these 'land cover costs' ranged from 10 – 100, which created a normalised scale between the three cost layers. Appropriate weightings for including cost factors are speculative; hence this study primarily focuses on the utility of the MC-LCP without this additional cost factor.

4.3 Modified Single-Flow-direction (MSF) model

Modelled flow in the MSF model has no physical basis and is solely a function of underlying terrain data, promoting its usage as a first-order assessment for GLOF flow path modelling (Huggel, 2004). It uses ArcGIS's D8 flow routing method and Path Distance tool, allowing flow to propagate downstream following the steepest descent, with up to 45° of lateral diversion. A methods workflow was outlined by Gruber et al. 2009. The MSF model can be stopped when a threshold run-out distance is reached based on the average channel slope from the source. However, for this study the flow exceeded the end of the study reach in all scenarios. The MSF model output reflects a qualitative likelihood of inundation, accounting

for increased flow resistance with lateral spread and distance downstream (Huggel et al., 2003).

4.4 HEC-RAS model

1D flood modelling was carried out in HEC-RAS 4.1.0, which has previously been used for modelling GLOF scenarios and reconstructing past events (e.g. Cenderelli and Wohl, 2003; Alho et al., 2005; Bajracharya et al., 2007; ICIMOD, 2011; Osti et al., 2013; Klimes et al., 2014), offering computational efficiency over long study reaches. Characteristically confined and topographically steep Himalayan reaches restrict the lateral inundation extent. If topographically unconfined and shallow, 2D models would better represent flow dynamics (e.g. Carrivick, 2006; Stains and Carrivick, 2015). In this study, 516 cross sections were added at 100-150 m intervals to capture downstream topographic and land cover changes (Figure 2b), and Manning's N roughness values were allocated to respective land covers following Chow (1959) and similar GLOF studies (e.g. Dussaillant et al., 2010; Jain et al. 2012). The HEC-GeoRAS extension in ArcGIS was used to extract cross section geometric and roughness data for use in HEC-RAS. Three scenarios of unsteady flow were evaluated, which represented a low, medium, and high magnitude event of 500 m^3 s^{-1}, 1000 m^3 s^{-1} and 2000 m^3 s^{-1} respectively. The scenarios are purely hypothetical and are derived from evaluation empirical regression equations relating an estimated lake volume for potentially dangerous glacial lakes in the catchment identified by the International Centre for Integrated Mountain Development (ICIMOD), to a potential peak discharge. The hypothetical hydrograph followed a linear rising and falling limb creating a triangular profile (e.g. Wang et al., 2012). The scenarios are referred to as profiles (Pf) one, two and three. The downstream boundary condition was set several kilometres below the town of Jakar (Figure 1) such that any errors arising from it would not affect the study reach (Brunner, 2010).

4.5 Flood implications

Finally, inundation extents and socio-economic impacts for each flood model and DEM combination were compared in order to assess the implications of using the different models and input DEMs. Downstream wetted width and flood depth were extracted for each cross section. Since the MC-LCP and MSF models do not produce a depth output, the channel width elevations of their flood extents were extracted and interpolated over the channel to estimate a depth surface, and this surface was differenced from the DEM.

Flood depths maps produced in HEC-RAS do not consider DEM uncertainty. Hence, a Monte Carlo based approach was used to communicate uncertainty within the HEC-RAS modelled flood extent. Here, the same DEM error model as from the MC-LCP was applied to the HEC-RAS depth map to evaluate whether each cell depth remained positive after iterative DEM uncertainty realisations. Since the process does not simulate a new flow after each terrain realisation (which would require a coupling between HEC-RAS and ArcGIS that was beyond the scope of this study), potential inundation outside of the initial flood extent was not considered,

5. Results

5.1 Inundated area

Differences in overall inundated area for each scenario represented a regional-scale model comparison that provides an indication of model stability with use of each DEM, and respective socio-economic and land cover inundation implications (Figure 7). The ALOS DEM was the only DEM producing a similar trend across all models. With the exception of the MC-LCP LC scenarios, the ALOS DEM consistently produced the smallest inundated area (Figure 7).

At a regional-scale, model sensitivity to DEM inputs is indicated by the inter-DEM inundated area range. Here, a smaller range indicates a lower dependence of the model on the terrain data used. The MC-LCP produced the smallest range at 0.85 km^2, followed by HEC-RAS with a minimum range considering all profiles of 2.48 km^2, and the MSF model at 4.86 km^2 (Table 4, Figure 7). Overall, the largest inundated areas were produced by the MC-LCP for all DEMs. However, these areas reduced when a land cover cost factor was introduced (Figure 7a). The inundated areas of the MSF model were most comparable to the HEC-RAS scenarios. HEC-RAS profiles 1 - 3 displayed the largest inundated range on the GDEM at 0.74 km^2, followed by the ALOS DEM and SRTM at 0.52 km^2 and 0.48 km^2 respectively (Figure 7b, Table 4).

[Figure 7 approximate location]

5.2 Inundated extents

Reporting total inundated area does not consider flow propagation, which was examined using downstream wetted width and visual inspection of flood extents between the models and for each DEM (Figure 8, 9). Wetted width variability due to DEM choice originates from the different initial products resolutions and hence variable river channel representation, and the DEM quality following pre-processing. Here, the ALOS and SRTM DEMs produced the smoothest downstream channel profiles following OPRN processing (Figure 2a). Notably the 'filled' SRTM and GDEM displayed a large positive elevation offset in the lower reach, which reflected the prevalence of artefacts in the original DEMs in this area (Figure 2a, b).

[Figure 8 & 9 approximate location]

The MC-LCP produced a consistently higher downstream wetted width (Figure 9) which reflects the overall larger inundated area (Figure 7a). Wetted width for the HEC-RAS Pf2 and the MSF models appeared similar, although it is evidently more variable downstream for

the HEC-RAS scenario (Figure 9b, c). A comparatively wider initial flood extent exists in all models between 0 - 10 km downstream, which was most prevalent in the HEC-RAS scenarios (Figure 9b). Similarly, all models suggested an increased inundation extent in the lower 10 km of the study reach, which was of greatest magnitude for the MSF model on the SRTM and GDEM (Figure 8c, 9c). This corresponded partly to where the valley bottom becomes wider and to where settlements are located (Figure 2).

Intra-model variability in downstream flood extent was generally greatest for the GDEM, whereas the ALOS and SRTM DEMs were more comparable and displayed less high magnitude peaks in wetted width. The high wetted width variability for the GDEM is most prominent in the HEC-RAS scenarios and for the MSF model (Figure 9b, c). In contrast to the comparatively continuous flood extent output by the MC-LCP (e.g. Figure 10a, d), downstream extent variability in the HEC-RAS output is highlighted by intermittent areas of ponding where water backwater effects are created by the confined channel reaches (Figure 10b, e).

[Figure 10 approximate location]

5.3 Depth characteristics

Downstream maximum depth displayed greatest variability for all models when run on the GDEM (Figure 9). The high incidence of low depth values for the MSF model (Figure 9c) corresponded to narrow modelled flood extents, where extracting a depth value beneath an interpolated surface exhibited greatest uncertainty. The physically-based HEC-RAS model produces the most robust indication of downstream depth variability. For the ALOS DEM, depth was generally below 20 m, which was always the case in the SRTM output (Figure 9a). In contrast, the GDEM scenario depth often exceeded 30 m and was over 40 m in some cases.

5.4 Inundated extent artefacts

Parallel flow artefacts representing finer scale uncertainty in flow routing were apparent in all MSF scenarios (e.g. Figure 8c, 10c, f). These artefacts were over 1 km long in some instances (e.g. Figure 10c). A notable contrast was also apparent in the lower reach for the MSF ALOS DEM, where a narrow flood extent contrasts with that of the SRTM and GDEM (Figure 8c, 9c). Artefacts of the OPRN pre-processing procedure were apparent in the HEC-RAS outputs where narrowly cut channels are apparent between areas of ponding (Figure 10b, e). In contrast, the MC-LCP produced a downstream continuum and represented flow 'braiding' around 'higher cost' channel features (e.g. Figure 10a, d).

5.5 Socio-economic implications

Examination of inundated land cover highlighted the prevalence of forest cover adjacent to the river channel and hence the importance of considering vegetation roughness in modelling scenarios (Figure 2b, 7). This forest cover also identifies potential debris input and damming hazard emanating from forested reaches, which was not considered in the modelling framework. The susceptibility to inundation of agricultural land in the lower reach is also highlighted for all scenarios (Figure 7). Comparing socio-economic vulnerabilities for the HEC-RAS output revealed a general increase in building and road inundation with higher magnitude flooding (Figure 7b), but inter-model comparisons revealed no clear association between socio-economic cost and inundated extent, highlighting the importance of evaluating local flow characteristics. For example, the MSF SRTM model predicted notably higher building and road inundation despite only representing 48 % of the inundated area depicted by the MC-LCP SRTM scenario (Figure 7a), since the MSF featured a large lateral extent in the populated lower reach. HEC-RAS outputs displayed the smallest range of building and road inundation across all scenarios, followed by the MC-LCP and the MSF model (Table 4).

5.6 Communication of risk

Each model pertains to a means of risk identification through either the number of times a grid cell was inundated, the depth of inundation at a cell, or a visual indication of inundation probability, for the MC-LCP, HEC-RAS, and MSF models respectively (Figure 10). Since the MSF model contains a function of downstream distance, a difference in inundation probability is only apparent in the vicinity of the start zone. Hence relative inundation probabilities cannot be meaningfully compared at finer scales for the MSF model, in contrast to the MC-LCP (Figure 10).

6. Discussion

The ability to conduct timely yet robust first-pass GLOF assessments is critical to direct further investigations, implement mitigation efforts, and derive hazard zonation, in response to climatic warming, glacial mass loss, and subsequent increased glacial lake development observed in the eastern Himalaya (Gardelle et al., 2011; Benn et al., 2012). Such first-pass assessments may represent the only means of GLOF flow routing where fine resolution topographic data are not available for robust hydrodynamic modelling. Additionally, a probabilistic GIS-based first-pass assessment is equally valuable prior to hydrodynamic modelling, since flow paths and areas of interest can be rapidly derived. The inter-model comparison presented here indicates that modelled flood extent, its dependence on topography, and subsequent societal impacts, can vary considerably due to the combination of model and DEM used.

The sensitivity of model output suggests that great caution should be exercised in data poor regions where such first-pass assessments may guide hazard zonation strategies, or where finer scale scenario implications are sought. Hence, although computationally more demanding (500 iterations for the Dig Tsho validation took four hours to run on a standard

laptop with a 2.20 GHz processor and 8 GB of RAM), the MC-LCP stochastic simulation based analysis provides a robust and informative indication of likely GLOF inundation with no increased implementation time investment required of the user.

The proposed stochastic simulation based analysis (MC-LCP) is able to consistently represent potential flood propagation without necessarily using a hydrologically correct DEM, which increases its utility in high relief catchments where artefacts are more likely in global DEM products (Pitman et al., 2013). Use of elevation and slope cost factors leads to standardised application between catchments and the model produces an inherent communication of uncertainty at the culmination of the GLOF process chain.

6.1 Topographic data

The 30 m ASTER GDEM V2 and 30 m SRTM (previously 90 m as used in this study) DEMs now represent the finest resolution open access elevation data. The GDEM and 90 m SRTM DEM products have seen usage in hydrodynamic modelling, with observed SRTM overestimation and GDEM underestimation of channel elevation (Wang et al., 2012). Although no GPS ground truth validation were available to this study, a similar observation of relatively higher elevation SRTM profiles was apparent for lengths of the study reach reported here (Figure 2). Studies deriving other topographic parameters have reported greater SRTM reliability (Frey and Paul, 2012; Mashimbye, 2014), but also that both DEMs cannot adequately represent a river channel in steep topography owing to irregular sensor sampling of the valley sides (Czubski et al., 2013; Pitman et al., 2013). SRTM 30 m data, which were made available for the Himalaya in early 2015, are likely to become widely used for first-pass assessments. The more comparable performance between the SRTM 90 m DEM and ALOS DEM shown in this study, suggests future use of the 30 m SRTM DEM will lead to greater convergence with finer resolution DEM products such as the ALOS DEM used here. This

likely reflects the single-pass data collection of the SRTM compared to the combination of scenes used in the GDEM.

Depression filling can be utilised to remove spurious sinks and peaks in the river channel; however, this is the most impacting approach since it can remove lengths of local minima which represent the river channel (Czubski et al., 2013). Therefore methods reducing terrain modification such as those implemented here are preferred (Lindsay and Creed, 2005), even though they bring their own demonstrated artefacts such as ‘cut’ river channels. The high downstream variability in extracted flood variables for the GDEM (Figure 9) represents the continued existence of sinks in the DEM following OPRN pre-processing (Figure 2a). The prevalence of sinks in the GDEM produces a notably variable flood extent for the HEC-RAS model (Figure 8b) and areas of flow ponding, which are separated by narrow channels where the OPRN algorithm has 'cut' (Figure 10b, e). The narrow channels reflect high relief regions of the study reach where DEM artefacts are likely to be most prevalent.

Overall the SRTM displays greater association with the finer resolution ALOS DEM, despite the positive channel elevation offset in some areas of the reach (Figure 2a). In contrast, Wang et al. (2012) found greater association between the GDEM and a finer resolution DEM when comparing the suitability of the GDEM and SRTM for GLOF assessment for a reach in Tibet. The greater channel gradient and high incidence of forest cover adjacent to the river channel in this study may explain the increased GDEM variability. Though both DEMs are surface models, the GDEM V2 represents a ten year fusion of data acquisition, whereas the SRTM dataset was collecting during an 11 day mission and coincided with leaf-off conditions for northern hemisphere forests (ASTER GDEM Validation Team, 2011).

6.2 Model comparison

The MSF model can be implemented quickly for several start sites, which increases its utility for regional assessments. However, sensitivity to DEM resolution and quality restricts local scale evaluation of flow routing (Huggel et al., 2003), as highlighted by linear artefacts and variability in inundated extent between DEMs of 4.86 km^2. This is especially evident in the lower reach of the GDEM and SRTM MSF scenarios where significant filling occurred (Figure 2a), leading to a notably larger extent compared to the ALOS DEM (Figure 8c). Elevation peaks in the channel profile further downstream leads to the 'fill' algorithm raising the upstream DEM cells to the height of this peak to allow continued flow propagation, hence creating an artificially flat and wider channel (Figure 2b). This demonstrates a notable sensitivity when applying the MSF to high relief reaches where such erroneous flood extents may be misinterpreted if applied on a regional scale, without finer scale flow path and DEM interrogation.

HEC-RAS scenarios demonstrated reduced sensitivity to DEM choice compared to the MSF model with a maximum inundation range between respective profiles of 2.48 km^2. The GDEM scenario produced the least consistent flood extent, followed by the SRTM and ALOS DEMs (Figure 8b, 9b). This extent variability is partly derived from issues when interpolating flood extent between cross sections for the high relief study reach, but is also linked to quality of the processed DEM used. Here, the GDEM displayed prominent erroneous peaks in the lower reach despite the OPRN processing (Figure 2a). This amplifies the ponding of water in the model where the reaches contract and expand. However, ponding was observed throughout the HEC-RAS output, where narrow reaches are encountered causing a natural ‘backlog’ of water (e.g. Carrivick et al., 2013). The sustained high-depth artefact for the HEC-RAS GDEM and SRTM scenarios at the end of the study reach (Figure 9b) is likely owing to the high relief and heavily forested channel here. Since the DEM

cannot adequately resolve the channel, this promotes a reverse profile and hence a build-up of water in the hydraulic model (Figure 9b). With a finer initial sampling resolution, the ALOS DEM is less sensitive to such sampling artefacts.

Where DEM data quality is an issue and filling causes widespread degradation of the DEM, as evidenced here, the MC-LCP still produces an acceptable flood extent comparable to the HEC-RAS scenarios. The MC-LCP generally produced the largest flood extent and hence downstream wetted width (Figure 8a, 9a). In the field of disaster mitigation, modelling the worst-case scenario is perhaps more justified than underestimation (Wang et al., 2012). Additionally, the MC-LCP model accounts for DEM uncertainty, hence the inundated extent represents the area that was considered a path of least resistance during the iterative terrain realisations.

Similar to the MSF, the MC-LCP model has no physical basis and does not consider flood magnitude, although the output could be classified into relative probability bands using the inundation frequency output (Figure 10a, d). This would mean that cells with a high inundation frequency are more susceptible to smaller flood events, whereas cells with a lower inundation frequency would be more susceptible to a higher magnitude flood. The MC-LCP is based on a subjective cost weighting of elevation difference from the channel, local slope, and allows for the inclusion of additional GIS layers such as land cover. However, that the former two factors are applicable to any DEM means that the MC-LCP's outputs are standardised between applications. The inclusion of a land cover cost using a reclassification of the Manning's N values used in HEC-RAS produced a lower inundated area (Figure 7a), owing to restricted divergence in the extensive forested reaches but increased divergence over agricultural and barren land. When investigating the impacts of future land use change on GLOF risk (e.g. Nussbaumer et al., 2014), the MC-LCP could therefore demonstrate how evolving land cover scenarios would modify the GLOF flow path.

Though still only acting as a first-pass assessment, the MC-LCP demonstrates increased utility at local scales where relative risks can be evaluated using the lateral inundation extent and frequency. The MC-LCP model also demonstrated the greatest stability between each DEM with a difference with an inundated area range of 0.85 km^2 (e.g. Figure 7a). Good agreement between the MC-LCP and geomorphic evidence of the Dig Tsho GLOF event lends further support to using this method to evaluate GLOF flow path propagation (Figure 6). Improved flow routing was a notable benefit in this study, where the linear artefacts inherent in the MSF output were over 1 km long in places (e.g. Figure 10c).

6.3. Socio-economic implications

Extracting the relative socio-economic implications of each scenario facilitates an evaluation of model choice and DEM sensitivities. Increasing flood magnitude HEC-RAS scenarios correspond with greater damage potential. However, since each model represents flow using a different technique, a greater flood extent does not necessarily equate to higher socio-economic implications (Figure 7). The MC-LCP uses a least cost path approach, the MSF requires the maintenance of flow direction, and HEC-RAS propagates open channel flow using 1D St. Venant equations. Hence differing flow patterns were expected. The MSF scenarios produced the greatest variation in this case, since the GDEM and SRTM scenarios displayed an exaggerated extent in the lower reach in response to using a filled DEM. In contrast, the MSF model appeared to under represent lateral divergence on the ALOS DEM (e.g. Figure 8c).

6.4 Communication of risk and uncertainty

The GLOF workflow often contains large uncertainties at each linkage, including dam breach formation and simulation (Osti and Egashira, 2009; Westoby et al., 2014); peak discharge and lake volume estimation (Huggel et al., 2002; Fujita et al., 2013); and the flood propagation

itself (Westoby et al., 2014). In addition, compounding factors exist such as debris entrainment, temporary damming, and the initiation of secondary landslides (Kuenza et al., 2010). Increased vulnerability and continued habitation of hazardous zones exists where communication and trust between local people, scientists, and policy makers is lacking (Carey, 2005). Modelling efforts that contain an inherent communication of uncertainty can therefore begin to bridge this gap at the expense only of increased computational processing time. Risk maps should represent a range of scenarios and an indication of confidence in each to avoid under or over representation. Although a transition towards coupling individual process-based modelling efforts of the GLOF workflow is desirable (Worni et al., 2014), such efforts are not feasible at regional-scales where first-pass assessments can provide an initial indication of risk.

The MC-LCP incorporates an uncertainty assessment and displays least sensitivity to DEM quality. Monte Carlo simulations implemented following a terrain realisation approach, which was adopted in the MC-LCP, can be utilised to derive confidence maps using the output of any hydrodynamic model and an estimate of DEM uncertainty. Alternatively, the approach can also introduce a stochastic element into flood mapping scenarios where other uncertainties exist in modelling the process chain. Retrospectively applying a DEM error model to the output of a hydrodynamic model (e.g. Figure 8d) allows an assessment of uncertainty within the modelled flood extent. However, this approach does not evaluate DEM cells outside of the initial input boundary, in contrast to Figure 8e. Considering DEM uncertainty when using hydrodynamic models such as HEC-RAS, requires DEM terrain realisations to be input for each model iteration. Such coupling was beyond the scope of this study but was undertaken manually for 10 iterations to provide a visual illustration and comparison with the MC-LCP extent (Figure 8e). These ‘fuzzy’ outputs (e.g. Figure 8d, e) deliver an enhanced decision support utility for subsequent inundation probability

interpretation, especially when using a lower quality dataset, or undertaking hazard zonation mapping.

7. Conclusions and further work

The utility of the MSF model to model basic GLOF flow path propagation is confirmed for a Himalayan study reach. However, the long reach length subdues any lateral interpretation of inundation probability and the requirement to use a 'filled' DEM can create a high incidence of parallel flow artefacts. These MSF artefacts were most apparent in the global DEM products but they also appeared in a 15 m resolution ALOS PRISM DEM.

The new MC-LCP approach developed as part of this study displayed improved flow routing compared to widely used MSF model, and displayed a stable flood extent, independent of the DEM used. This independence of model performance to DEM product is likely to be important in other confined and high relief Himalayan reaches, where the GDEM and SRTM suffer with artefacts of poor channel delineation. Model scenarios using the SRTM produced more consistent flood characteristics in all cases, in line with those scenarios using the finer resolution ALOS DEM. This is likely to be further improved as 30 m SRTM data become commonly used for first-pass assessments.

More widely, this study has shown that caution should be exercised in data poor regions where remote sensing based first-pass assessments may guide hazard zonation strategies, or where local scale scenario implications are sought, since the socio-economic implications of contrasting flow models and DEMs can diverge notably. Nevertheless, we have shown that the MC-LCP model is able to represent the lateral inundation of the most vulnerable terrain in to a flood event, and that inundation extent is comparable to that predicted with use of a 1D hydrodynamic model. The user-customisable error model in the MC-LCP facilitates uncertainty assessments even if DEM error is low, since DEM noise perturbation could

represent other process chain uncertainties. The stochastic approach demonstrated here could benefit from GIS applications of circuit theory when applied to multiple catchments simultaneously. Circuit theory can similarly replicate least cost paths between two nodes over a cost layer; however, owing to enhanced algorithm development, these techniques can produce multiple pathway corridors with greatly reduced processing time (McRae et al., 2008). An example is provided in the supplementary information (Figure S1).

Further development of the model could incorporate a downstream distance decay function to represent flood attenuation. This decay function would be more informative than a simple slope-dependant model cut-off for Himalayan reaches, where the potential flood travel distance is extensive. The inherent incorporation and 'fuzzy boundary' communication of uncertainty improves the utility of the MC-LCP when dealing with a hazard for which the process chain contains large and propagating uncertainties. The optional inclusion of additional cost layers such as land cover, offers increased analytical ability within the model framework. In addition, a simple calibration between the modelled DEM cost layers and high water marks of a past event could further improve the utility of this initial assessment technique since the cost layer itself could give an indication of relative inundation extents, without requiring model iterations.

In summary, we suggest that the key advantages of the MC-LCP approach are as follows:

- It produces a flood inundation extent which represents DEM uncertainty.
- Flood inundation frequency allows an assessment of relative risk at a local scale.
- It is least sensitive to DEM choice.
- Additional cost factors such as land cover can be incorporated.
- It has low data requirements and a quick setup time.

Acknowledgements

ALOS PRISM data were provided through the 4th ALOS Research Announcement for ALOS-2 under agreement 1008 (Quincey). Matt Westoby and another anonymous reviewer are thanked for detailed comments on the earlier manuscript of this paper.

References

Alho, P. Russell, A.J. Carrivick, J.L. and Käyhkö, J. 2005. Reconstruction of the largest Holocene jökulhlaup within Jökulsá á Fjöllum, NE Iceland. *Quaternary Science Reviews.* **24**(22), pp.2319-2334.

ASTER GDEM Validation Team. 2011. ASTER Global Digital Elevation Model Version 2 Summary of Validation Results. [Online]. [Accessed 05 June 2014]. Available from: https://lpdaacaster.cr.usgs.gov/GDEM/Summary_GDEM2_validation_report_final.pdf

Bajracharya, S. R. Mool, P. K. and Shrestha, B. R. 2007. Impact of Climate Change on Himalayan Glaciers and Glacial Lakes: Case Studies on GLOF and Associated Hazards in Nepal and Bhutan. [Online]. Kathmandu: ICIMOD. [Accessed 13 May 2014]. Available from: http://lib.icimod.org/record/22442/files/attachment_169.pdf

Benn, D.I. Bolch, T. Hands, K. Gulley, J. Luckman, A. Nicholson, L.I. Quincey, D. Thompson, S. Toumi, R. and Wiseman, S. 2012. Response of debris-covered glaciers in the Mount Everest region to recent warming, and implications for outburst flood hazards. *Earth-Science Reviews*. **114**(1–2), pp.156-174.

Berthier, E.Arnaud, Y.Kumar, R.Ahmad, S.Wagnon, P. and Chevallier, P. 2007. Remote sensing estimates of glacier mass balances in the Himachal Pradesh (Western Himalaya, India). *Remote Sensing of Environment.* **108**(3), pp.327-338.

1 Berthier, E.Arnaud, Y.Vincent, C. and Remy, F. 2006. Biases of SRTM in high-mountain
2 areas: Implications for the monitoring of glacier volume changes. *Geophysical*
3 *Research Letters.* **33**(8).

4 Bolch, T. Peters, J. Yegorov, A. Pradhan, B. Buchroithner, M. and Blagoveshchensky,
5 V.2011. Identification of potentially dangerous glacial lakes in the northern Tien Shan.
6 *Natural Hazards*. **59**(3), pp.1691-1714.

7 Brunner, G.W. 2010. HEC-RAS river analysis system user's manual. [Online]. California: US
8 Army Corps of Engineers. [Accessed 19 June 2014]. Available from:
9 http://www.hec.usace.army.mil/software/hec-ras/documentation/HEC-
10 RAS_4.1_Users_Manual.pdf.

11 Byers, A. McKinney, D. Somos-Valenzuela, M. Watanabe, T. and Lamsal, D. 2013. Glacial
12 lakes of the Hinku and Hongu valleys, Makalu Barun National Park and Buffer Zone,
13 Nepal. *Natural Hazards*. **69**(1), pp.115-139.

14 Carey, M. 2005. Living and dying with glaciers: people's historical vulnerability to
15 avalanches and outburst floods in Peru. *Global and Planetary Change.* **47**(2–4),
16 pp.122-134.

17 Carlisle, B.H. 2005. Modelling the Spatial Distribution of DEM Error. *Transactions in GIS*.
18 **9**(4), pp.521-540.

19 Carrivick, J.L. 2006. Application of 2D hydrodynamic modelling to high-magnitude outburst
20 floods: An example from Kverkfjöll, Iceland. *Journal of Hydrology*. **321**(1–4), pp.187-
21 199.

22 Carrivick, J.L. and Tweed, F.S. 2013. Proglacial lakes: character, behaviour and geological
23 importance. *Quaternary Science Reviews*. **78**, pp.34-52.

1 Carrivick, J. L., Turner, A. G., Russell, A. J., Ingeman-Nielsen, T., & Yde, J. C. 2013.
2 Outburst flood evolution at Russell Glacier, western Greenland: effects of a bedrock
3 channel cascade with intermediary lakes. *Quaternary Science Reviews*. **67**, pp.39-58.

4 Cenderelli, D.A. and Wohl, E.E. 2001. Peak discharge estimates of glacial-lake outburst
5 floods and "normal" climatic floods in the Mount Everest region, Nepal.
6 *Geomorphology*. **40**(1–2), pp.57-90.

7 Chow, V.T. 1959. Open-Channel Hydraulics. New York: McGraw-Hill Book Co.

8 Center for Research in Water Resources. 2013. *Optimized Pit Removal* [Online]. [Accessed
9 05 June 2014]. Available from: http://tools.crwr.utexas.edu/

10 Czubski, K.Kozak, J. and Kolecka, N. 2013. Accuracy of SRTM-X and ASTER Elevation
11 Data and its Influence on Topographical and Hydrological Modeling Case Study of
12 the Pieniny Mts. in Poland. *International Journal of Geoinformatics* **9**(2), pp.7-14.

13 Dussaillant, A. Benito, G. Buytaert, W. Carling, P. Meier, C. and Espinoza, F. 2010.
14 Repeated glacial-lake outburst floods in Patagonia: an increasing hazard? *Natural*
15 *Hazards.* **54**(2), pp.469-481.

16 Emmer, A. and Vilímek, V. 2013. Review Article: Lake and breach hazard assessment for
17 moraine-dammed lakes: an example from the Cordillera Blanca (Peru). *Nat. Hazards*
18 *Earth Syst. Sci*. **13**(6), pp.1551-1565.

19 Endreny, T.A. and Wood, E.F. 2001. Representing elevation uncertainty in runoff modelling
20 and flowpath mapping. *Hydrological Processes*. **15**(12), pp.2223-2236.

21 Fisher, P.F. and Tate, N.J. 2006. Causes and consequences of error in digital elevation
22 models. *Progress in Physical Geography*. **30**(4), pp.467-489.

Frey, H. Haeberli, W. Linsbauer, A. Huggel, C. and Paul, F. 2010. A multi-level strategy for anticipating future glacier lake formation and associated hazard potentials. *Natural Hazards and Earth System Sciences*. **10**(2), pp.339-352.

Frey, H. and Paul, F. 2012. On the suitability of the SRTM DEM and ASTER GDEM for the compilation of topographic parameters in glacier inventories. *International Journal of Applied Earth Observation and Geoinformation.* **18**, pp.480-490.

Fujita, K. Sakai, A. Takenaka, S. Nuimura, T. Surazakov, A.B. Sawagaki, T. and Yamanokuchi, T. 2013. Potential flood volume of Himalayan glacial lakes. *Natural Hazards and Earth System Sciences.* **13**(7), pp.1827-1839.

Gardelle, J.Arnaud, Y. and Berthier, E. 2011. Contrasted evolution of glacial lakes along the Hindu Kush Himalaya mountain range between 1990 and 2009. *Global and Planetary Change.* **75**(1–2), pp.47-55.

Gatziolis, D. and Fried, J.S. 2004. Adding Gaussian noise to inaccurate digital elevation models improves spatial fidelity of derived drainage networks. *Water Resources Research*. **40**(2), pp.1-13.

Ghimire, M. 2005. Review of Studies on Glacier Lake Outburst Floods and Associated Vulnerability in the Himalayas. *Himalayan Review*. **35-36**, pp.49-64.

Gichamo, T.Z. Popescu, I. Jonoski, A. and Solomatine, D. 2012. River cross-section extraction from the ASTER global DEM for flood modeling. *Environmental Modelling & Software*. **31**, pp.37-46.

Gilani, H. Shrestha, H.L. Murthy, M.S. Phuntso, P. Pradhan, S. Bajracharya, B. and Shrestha, B. 2014 forthcoming. Decadal land cover change dynamics in Bhutan. *J Environ Management. pp.1-10.*

Gruber, S. Huggel, C. and Pike, R. 2009. Modelling mass movements and landslide susceptibility. In: Hengl, T. and Reuter, H.I. *Geomorphometry concepts, software, applications*. Amsterdam: Elsevier, pp.527-550.

Gruber, F.E. and Mergili, M. 2013. Regional-scale analysis of high-mountain multi-hazard and risk indicators in the Pamir (Tajikistan) with GRASS GIS. *Nat. Hazards Earth Syst. Sci.* **13**(11), pp.2779-2796.

Hayakawa, Y.S. Oguchi, T. and Lin, Z. 2008. Comparison of new and existing global digital elevation models: ASTER G-DEM and SRTM-3. *Geophysical Research Letters*. **35**(17), pp1-5.

Hebeler, F. and Purves, R.S. 2009. The influence of elevation uncertainty on derivation of topographic indices. *Geomorphology*. **111**(1–2), pp.4-16.

Huggel, C. Kääb, A. Haeberli, W. Teysseire, P. and Paul, F. 2002. Remote sensing based assessment of hazards from glacier lake outbursts: a case study in the Swiss Alps. *Canadian Geotechnical Journal*. **39**(2), pp.316-330.

Huggel, C. Kääb, A. Haeberli, W. and Krummenacher, B. 2003. Regional-scale GIS-models for assessment of hazards from glacier lake outbursts: evaluation and application in the Swiss Alps. *Nat. Hazards Earth Syst. Sci*. **3**(6), pp.647-662.

Huggel, C. 2004. *Assessment of glacial hazards based on remote sensing and GIS modeling.* PhD thesis. University of Zurich.

Huggel, C.Haeberli, W.Kaab, A.Bieri, D. and Richardson, S. 2004a. An assessment procedure for glacial hazards in the Swiss Alps. *Canadian Geotechnical Journal.* **41**(6), pp.1068-1083.

Huggel, C., Kaab, A. and Salzmann, N. 2004b. GIS-based modelling of glacial hazards and their interactions using Landsat-TM and IKONOS imagery. *Norsk Geografisk Tidsskrift–Norwegian Journal of Geography*. **58**(2), pp.61– 73.

International Centre for Integrated Mountain Development. 2011. Glacial lakes and glacial lake outburst floods in Nepal. [Online]. Kathmandu: ICIMOD. [Accessed 14 May 2014]. Available from: http://www.icimod.org/dvds/201104_GLOF/reports/final_report.pdf

Iribarren Anacona, P.Norton, K.P. and Mackintosh, A. 2014. Moraine-dammed lake failures in Patagonia and assessment of outburst susceptibility in the Baker Basin. *Nat. Hazards Earth Syst. Sci.* **14**(12), pp.3243-3259.

Jain, S. Lohani, A. Singh, R.D. Chaudhary, A. and Thakural, L.N. 2012. Glacial lakes and glacial lake outburst flood in a Himalayan basin using remote sensing and GIS. *Natural Hazards*. **62**(3), pp.887-899.

Jamtsho, T. Chakarvarty, U. 2012. World SHP Development Report: Bhutan. [Online]. [Accessed 8th April 2014]. Available from: http://www.inshp.org/Img_Lib/UploadImg/20127309474769.pdf

Kaab, A. 2005. Combination of SRTM3 and repeat ASTER data for deriving alpine glacier flow velocities in the Bhutan Himalaya. *Remote Sensing of Environment*. **94**(4), pp.463-474.

Klimes, J. Benesova, M. Vilimek, V. Bouska, P. and Cochachin Rapre, A. 2014. The reconstruction of a glacial lake outburst flood using HEC-RAS and its significance for future hazard assessments: an example from Lake 513 in the Cordillera Blanca, Peru. *Natural Hazards*. **71**(3), pp.1617-1638.

Koike, T. and Takenaka, S. 2012. Scenario Analysis on Risks of Glacial Lake Outburst Floods on the Mangde Chhu River, Bhutan. *Global Environmental Research*. **16**, pp.41-49.

Kolecka, N. and Kozak, J. 2014. Assessment of the Accuracy of SRTM C- and X-Band High Mountain Elevation Data: a Case Study of the Polish Tatra Mountains. *Pure and Applied Geophysics*. **171**(6), pp.897-912.

Komori, J. 2008. Recent expansions of glacial lakes in the Bhutan Himalayas. *Quaternary International*. **184**(1), pp.177-186.

Kuenza, K. Dorji, Y. and Dorji, W. 2010. Landslides in Bhutan. *SAARC workshop on landslide risk management in South Asia, 11-12 May 2010, Thimpu, Bhutan*. pp. 73-80. [Online]. [Accessed 20 May 2014]. Available from: http://www.preventionweb.net/english/professional/publications/v.php?id=14793

Lindsay, J.B. and Creed, I.F. 2005. Removal of artifact depressions from digital elevation models: towards a minimum impact approach. *Hydrological Processes.* **19**(16), pp.3113-3126.

Lindsay, J.B. and Evans, M.G. 2008. The influence of elevation error on the morphometrics of channel networks extracted from DEMs and the implications for hydrological modelling. *Hydrological Processes*. **22**(11), pp.1588-1603.

Mashimbye, Z.E., De Clercq, W.P., Van Niekerk, A. 2014. An evaluation of digital elevation models (DEMs) for delineating land components. *Geoderma.* **213**, pp.312-319.

McKillop, R. and Clague, J. 2007. A procedure for making objective preliminary assessments of outburst flood hazard from moraine-dammed lakes in southwestern British Columbia. *Natural Hazards*. **41**(1), pp.131-157.

McRae, B.H.Dickson, B.G.Keitt, T.H. and Shah, V.B. 2008. Using Circuit Theory to Model Connectivity in Ecology, Evolution, and Conservation. *Ecology.* **89**(10), pp.2712-2724.

Meenawat, H. and Sovacool, B. 2011. Improving adaptive capacity and resilience in Bhutan. *Mitigation and Adaptation Strategies for Global Change*. **16**(5), pp.515-533.

Melles, S.J.Jones, N.E.Schmidt, B. and Rayfield, B. 2011. A least-cost path approach to stream delineation using lakes as patches and a digital elevation model as the cost surface. *Procedia Environmental Sciences.* **7**, pp.240-245.

Mergili, M. and Schneider, J.F. 2011. Regional-scale analysis of lake outburst hazards in the southwestern Pamir, Tajikistan, based on remote sensing and GIS. *Nat. Hazards Earth Syst. Sci*. **11**(5), pp.1447-1462.

Mergili, M.Müller, J.P. and Schneider, J.F. 2013. Spatio-temporal development of high-mountain lakes in the headwaters of the Amu Darya River (Central Asia). *Global and Planetary Change.* **107**, pp.13-24.

Mool, P.K. Wangda, D. Bajracharya, S.R. Kunzang, K. Gurung, D.R. and Joshi, S.P. 2001. Inventory of glaciers, glacial lakes, and glacial lake outburst floods: Monitoring and early warning systems in the Hindu Kush-Himalayan region – Bhutan. [Online]. Kathmandu: ICIMOD. [Accessed 13 May 2014]. Available from: http://www.preventionweb.net/files/2370_InventoryGlaciers.pdf

National Environment Commission. 2009. Strategizing climate change for Bhutan. [Online]. [Accessed 26 March 2014]. Available from: http://www.rrcap.ait.asia/nsds/uploadedfiles/file/bhutan.pdf

Nie, Y. Liu, Q. and Liu, S. 2013. Glacial Lake Expansion in the Central Himalayas by Landsat Images, 1990–2010. *PLoS ONE*. **8**(12), pp.1-8.

Nussbaumer, S.Schaub, Y.Huggel, C. and Walz, A. 2014. Risk estimation for future glacier lake outburst floods based on local land-use changes. *Nat. Hazards Earth Syst. Sci.* **14**(6), pp.1611-1624.

Osti, R. and Egashira, S. 2009. Hydrodynamic characteristics of the Tam Pokhari glacial lake outburst flood in the Mt. Everest region, Nepal. *Hydrological Processes*. **23**(20), pp.2943-2955.

Osti, R.Egashira, S. and Adikari, Y. 2013. Prediction and assessment of multiple glacial lake outburst floods scenario in Pho Chu River basin, Bhutan. *Hydrological Processes.* **27**(2), pp.262-274.

Paul, F. 2008. Calculation of glacier elevation changes with SRTM: is there an elevation-dependent bias? *Journal of Glaciology.* **54**(188), pp.945-946.

Pitman, E.B. Patra, A.K. Kumar, D. Nishimura, K. and Komori, J. 2013. Two phase simulations of glacier lake outburst flows. *Journal of Computational Science*. **4**(1-2), pp.71-79.

Rexer, M. and Hirt, C. 2014. Comparison of free high resolution digital elevation data sets (ASTER GDEM2, SRTM v2.1/v4.1) and validation against accurate heights from the Australian National Gravity Database. *Australian Journal of Earth Sciences*. **61**(2), pp.213-226.

Richardson, S.D. and Reynolds, J.M. 2000. An overview of glacial hazards in the Himalayas. *Quaternary International*. **65–66**, pp.31-47.

Rusli, N. Majid, M.R. and Din, A.H.M. 2014. Google Earth's derived digital elevation model: A comparative assessment with Aster and SRTM data. *IOP Conference Series: Earth and Environmental Science*. **18**(1), pp.1-6.

1 Sanders, B.F. 2007. Evaluation of on-line DEMs for flood inundation modeling. *Advances in*
2 *Water Resources*. **30**(8), pp.1831-1843.

3 Shortridge, A. and Messina, J. 2011. Spatial structure and landscape associations of SRTM
4 error. *Remote Sensing of Environment*. **115**(6), pp.1576-1587.

5 Soille, P. 2004. Optimal removal of spurious pits in grid digital elevation models. *Water*
6 *Resources Research.* **40**(12), pp.1-9.

7 Staines, K.E.H. and Carrivick, J.L. 2015. Geomorphological impact and morphodynamic
8 effects on flow conveyance of the 1999 jökulhlaup at Sólheimajökull, Iceland. *Earth*
9 *Surface Processes and Landforms.* doi: 10.1002/esp.3750

10 Sun, G.Ranson, K.J.Khairuk, V.I. and Kovacs, K. 2003. Validation of surface height from
11 shuttle radar topography mission using shuttle laser altimeter. *Remote Sensing of*
12 *Environment*. **88**(4), pp.401-411.

13 Takenaka, S. Satoh, T. and Lhamo, S. 2012. A Social Survey for GLOF Disaster Mitigation
14 in Bhutan. *Global Environmental Research*. **16**, pp.77-82.

15 United Nations Disaster Management Team. 2005. Disaster Management Analysis in Bhutan.
16 [Online]. [Accessed 14 May 2014]. Available from:
17 http://www.raonline.ch/pages/bt/pdf/UNDMT_BThazards0502.pdf

18 Veregin, H. 1997. The Effects of Vertical Error in Digital Elevation Models on the
19 Determination of Flow-path Direction. *Cartography and Geographic Information*
20 *Systems*. **24**(2), pp.67-79.

21 Wangdi, N. and Kusters, K. 2012. The costs of adaptation in Punakha, Bhutan: Loss and
22 damage associated with changing monsoon patterns. [Online]. [Accessed 13 May 2014].
23 Available from: http://www.lossanddamage.net/download/6902.pdf

Wang, W. Yang, X. and Yao, T. 2012. Evaluation of ASTER GDEM and SRTM and their suitability in hydraulic modelling of a glacial lake outburst flood in southeast Tibet. *Hydrological Processes*. **26**(2), pp.213-225.

Watanbe, T. and Rothacher, D. 1996. The 1994 Lugge Tsho Glacial Lake Outburst Flood, Bhutan Himalaya. *Mountain Research and Development*. **16**(1), pp.77-81.

Wechsler, S.P. 2007. Uncertainties associated with digital elevation models for hydrologic applications: a review. *Hydrol. Earth Syst. Sci.* **11**(4), pp.1481-1500.

Westoby, M.J. Brasington, J. Glasser, N.F. Hambrey, M.J. Reynolds, J.M. Hassan, M.A.A.M. and Lowe, A. 2015. Numerical modelling of glacial lake outburst floods using physically based dam-breach models. *Earth Surf. Dynam.* **3**(1), pp.171-199.

Westoby, M.J. Glasser, N.F. Brasington, J. Hambrey, M.J. Quincey, D.J. and Reynolds, J.M. 2014. Modelling outburst floods from moraine-dammed glacial lakes. *Earth-Science Reviews*. **134**, pp.137-159.

Worni, R. Huggel, C. Clague, J.J. Schaub, Y. and Stoffel, M. 2014. Coupling glacial lake impact, dam breach, and flood processes: A modeling perspective. *Geomorphology*. **224**, pp.161-176.

Worni, R. Huggel, C. and Stoffel, M. 2012. Glacial lakes in the Indian Himalayas--from an area-wide glacial lake inventory to on-site and modeling based risk assessment of critical glacial lakes. *Sci Total Environ.* **468-469**, pp.S71-84.

Zandbergen, P.A. 2011. Error Propagation Modeling for Terrain Analysis using Dynamic Simulation Tools in ArcGIS Modelbuilder. *Geomorphometry*. [Online]. pp.57-60. [Accessed 19 June 2014]. Available from: http://www.geomorphometry.org/system/files/Zandbergen2011geomorphometry.pdf

Tables:

Table 1. Relative elevation differences between downstream river channel profiles from each DEM.

DEM absolute mean difference and (standard deviation) (m)	GDEM OPRN	SRTM OPRN	ALOS FILLED	GDEM FILLED	SRTM FILLED
ALOS OPRN	17.4 (21.8)	13.1 (12.9)	7.5 (18.8)	24.7 (23.0)	18.4 (17.6)
GDEM OPRN	-	18.7 (18.1)	20.2 (25.0)	23.4 (20.5)	22.7 (28.7)
SRTM OPRN	-	-	12.4 (19.7)	18.3 (20.3)	5.6 (10.4)

Table 2. Comparison of terrain modification resulting from 'fill' and 'OPRN' DEM processing.

DEM	Fill			OPRN		
	Modified cells (%)	Mean fill (m)	Max fill (m)	Modified cells (%)	Mean fill/ cut (m)	Max fill/ cut (m)
GDEM	4.9	21.2	119.0	1.34	3.7/ -9.4	41.5/ -81.6
SRTM	2.4	16.0	52.0	0.49	2.3/ -5.6	14.3/ -45.0
ALOS*	7.8	53.2	1386.8	2.55	17.4/ -21.32	953.0/ -598.5

Reported statistics highlight the difference between DEM pre-processing algorithms for each study reach DEM, not exclusively the river channel environment. *ALOS statistics therefore include large artefacts of the DEM generation procedure where areas of cloud were present on adjacent valley slopes

1 Table 3. Validation of the MC-LCP model against geomorphic evidence of the 1985 Dig
2 Tsho GLOF

Reach ID	GLOF reach area derived from geomorphic evidence (m^2)*	MC-LCP intersection with geomorphic evidence (m^2)**	GLOF extent accounted for by the MC-LCP (%)
L1	181942	132615	73
L2	115889	99265	86
L4	137546	105172	76
L5	23652	19667	83
L7	16872	14805	88
L8	49967	31162	62

* Mapped by Cenderelli and Wohl (2001)

**Shown in Figure 6

3

4 Table 4. Inundated extent and socio-economic implications for each model scenario.

Scenario	Inundated extent (km^2)	Inter-DEM extent range (km^2)	Building inundation	Road inundation (km)	Socio-economic range (buildings/ road (km))
MC-LCP GDEM 500	9.68		107	6.59	
MC-LCP SRTM 500	10.46	0.85	118	9.03	34/ 2.45
MC-LCP ALOS 500	9.61		84	6.85	
MC-LCP GDEM LC 500*	6.97		138	5.94	
MC-LCP SRTM LC 500*	8.03	1.06	144	6.54	16/ 2.49
MC-LCP ALOS LC 500*	7.88		128	8.43	
MSF GDEM	7.81		246	16.91	
MSF SRTM	5.46	4.86	145	12.14	241/ 16.03
MSF ALOS	2.94		5	0.88	
HEC-RAS GDEM Pf1	6.35		53	4.05	
HEC-RAS GDEM Pf2	6.86	2.48**	56	4.46	31/ 0.72**
HEC-RAS GDEM Pf3	7.09		56	4.37	

HEC-RAS SRTM Pf1	5.29		36	4.25	1
HEC-RAS SRTM Pf2	5.65		37	4.35	2
HEC-RAS SRTM Pf3	5.77		37	4.65	3
HEC-RAS ALOS Pf1	3.86		11	3.20	4
HEC-RAS ALOS Pf2	4.18		20	3.56	5
HEC-RAS ALOS Pf3	4.38		25	3.93	6
* MC-LCP scenarios incorporating a land cover cost factor.					7
**Minimum inter-DEM range considering all HEC-RAS scenario profiles. Individual profile ranges are given below:					8
Pf1 range: 2.48 km^2, 42 buildings, & 1.06 km of road.					
Pf2 range: 2.68 km^2, 36 buildings, & 0.90 km of road.					9
Pf3 range: 2.71 km^2, 31 buildings, & 0.72 km of road.					
					10

Figure captions

Figure 1. Location of the Chamkar Chu basin study reach within Bhutan and the potentially hazardous lakes identified by Mool et al. (2001).

Figure 2. Study reach overview. (a) Channel elevation profiles for each Optimised Pit Removal Net (OPRN) processed and filled DEM. (b) Example cross sections from the HEC-RAS model demonstrating the difference between the OPRN and filled DEMs.

Figure 3. Study workflow outlining the model evaluation procedure for the hypothetical inundation scenarios.

Figure 4. Components and process of the MC-LCP model.

Figure 5. Evaluation of the MC-LCP inundated area stability with increasing number of model iterations

Figure 6. Validation of the MC-LCP model against the field-measured flood extent of the 1985 Dig Tsho GLOF using the ASTER GDEM v2. The six reaches are those numbered and reported by Cenderelli and Wohl (2001).

Figure 7. Inundated area graphs for (a) GIS-based models, and (b) HEC-RAS scenarios, where profiles 1-3 represent increasing magnitude flood scenarios.

Figure 8. (a-c) Example flood extent maps for the application of each model to respective DEMs in the lower reach. The medium magnitude scenario (Pf2) extents are shown for the HEC-RAS model. (d) Inundation confidence map within one HEC-RAS output produced by classifying positive flood depth during 500 stochastic terrain realisations on the GDEM. Note that this method does not consider inundation uncertainty outside of the initial input boundary. (e) Inundation frequency derived by manually inputting ten terrain realisations into HEC-RAS simulations run on the GDEM. This method allows DEM uncertainty to be considered during each HEC-RAS simulation. The MC-LCP extent for the GDEM is shown for comparison.

Figure 9. Wetted width and maximum depth for the MC-LCP (a), HEC-RAS Profile 2 (b), and MSF (c) models. Maximum MSF depth (c) is plotted on a different scale. (d) The inter-profile difference for each HEC-RAS DEM scenario.

Figure 10. Model output comparison for an upper reach (a-c) and lower reach featuring the town of Jakar (d-f).

Figure S1. Comparison of the MC-LCP and CIRCUITSCAPE outputs using the SRTM. The fuzzy outputs are classified to single values representing the maximum modelled flood extent. 20 m contour intervals are shown with 100 m index contours.

Figure 1

Click here to download high resolution image

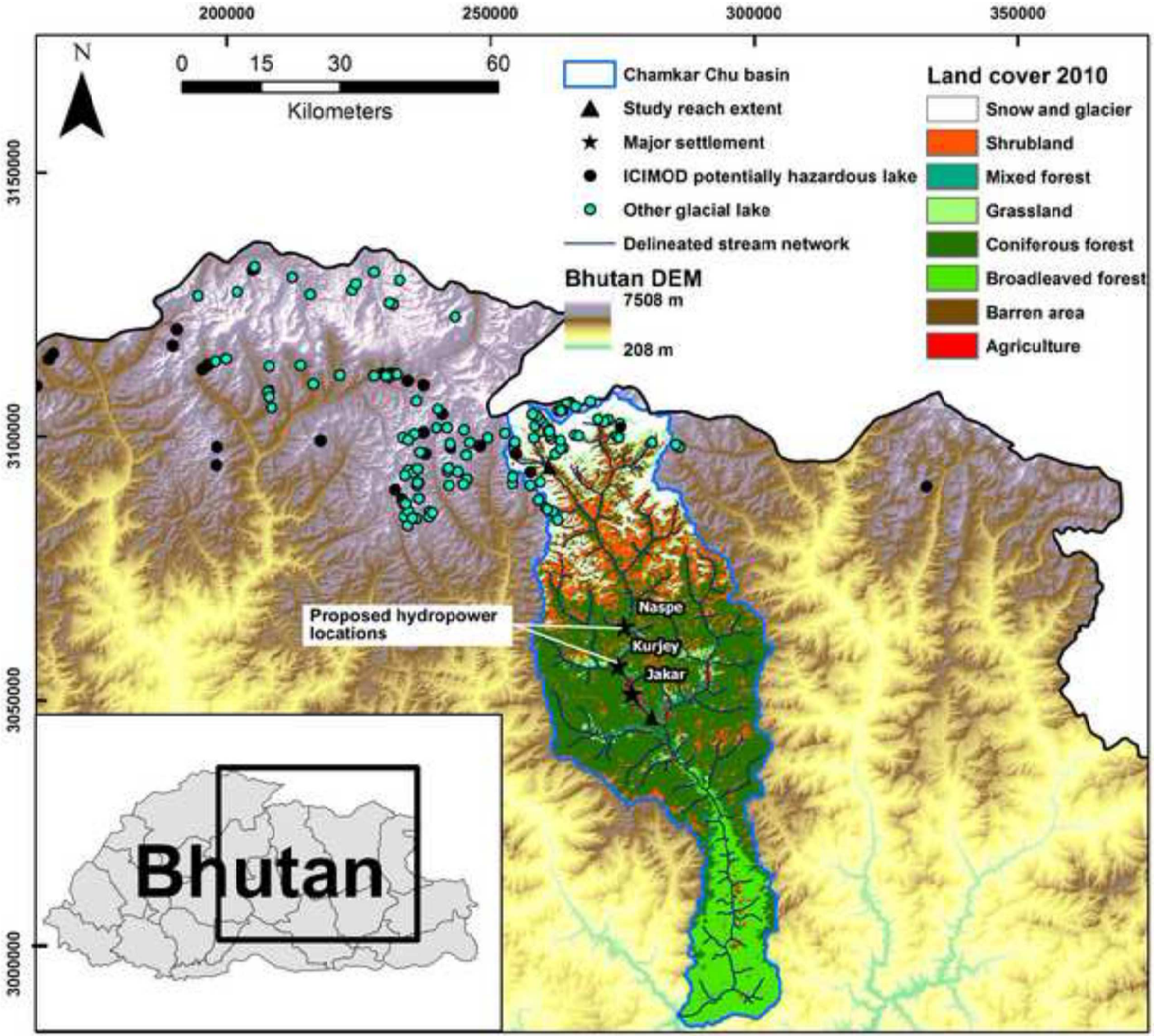

Figure 2

Click here to download high resolution image

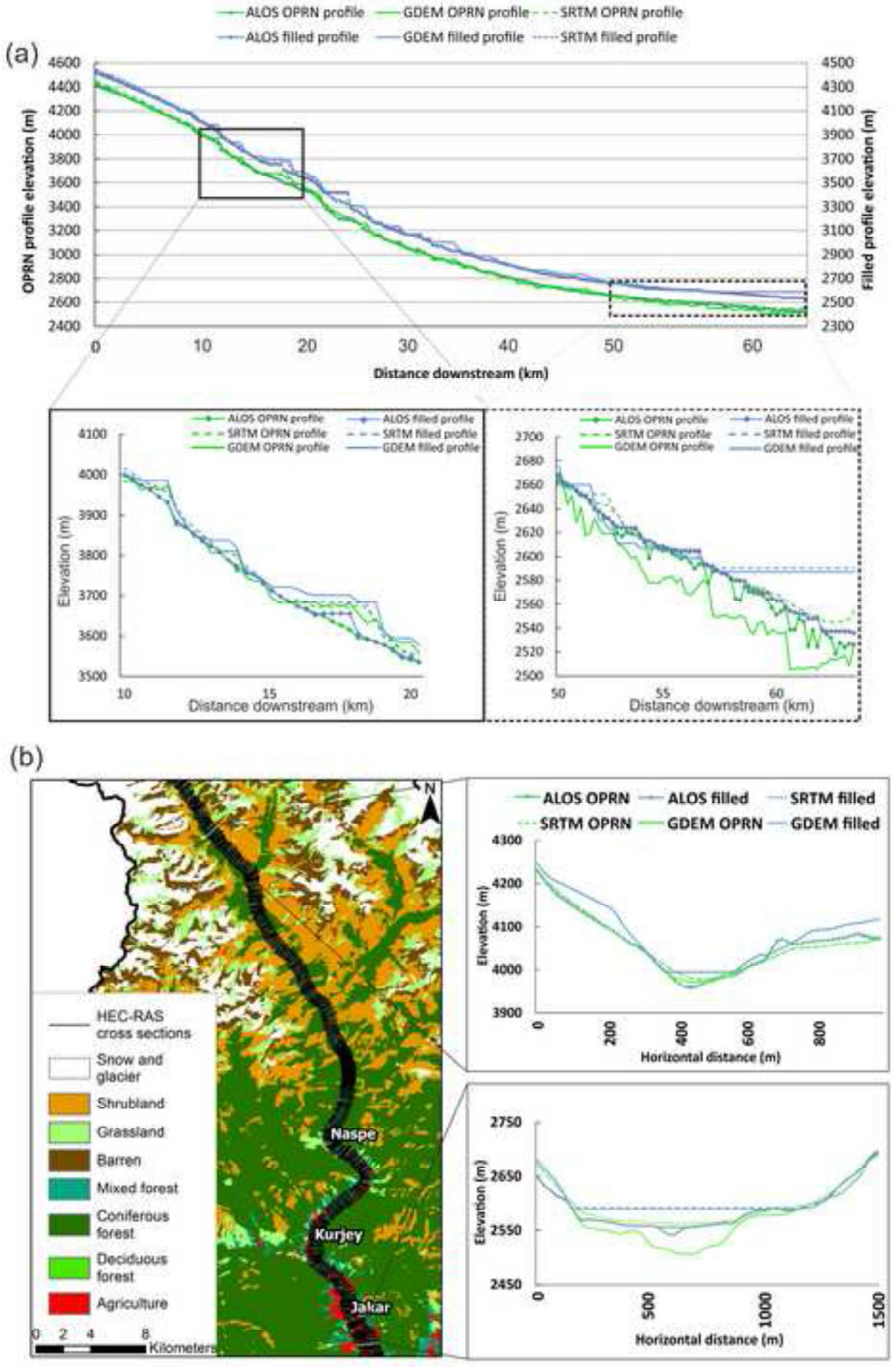

Figure 3
Click here to download high resolution image

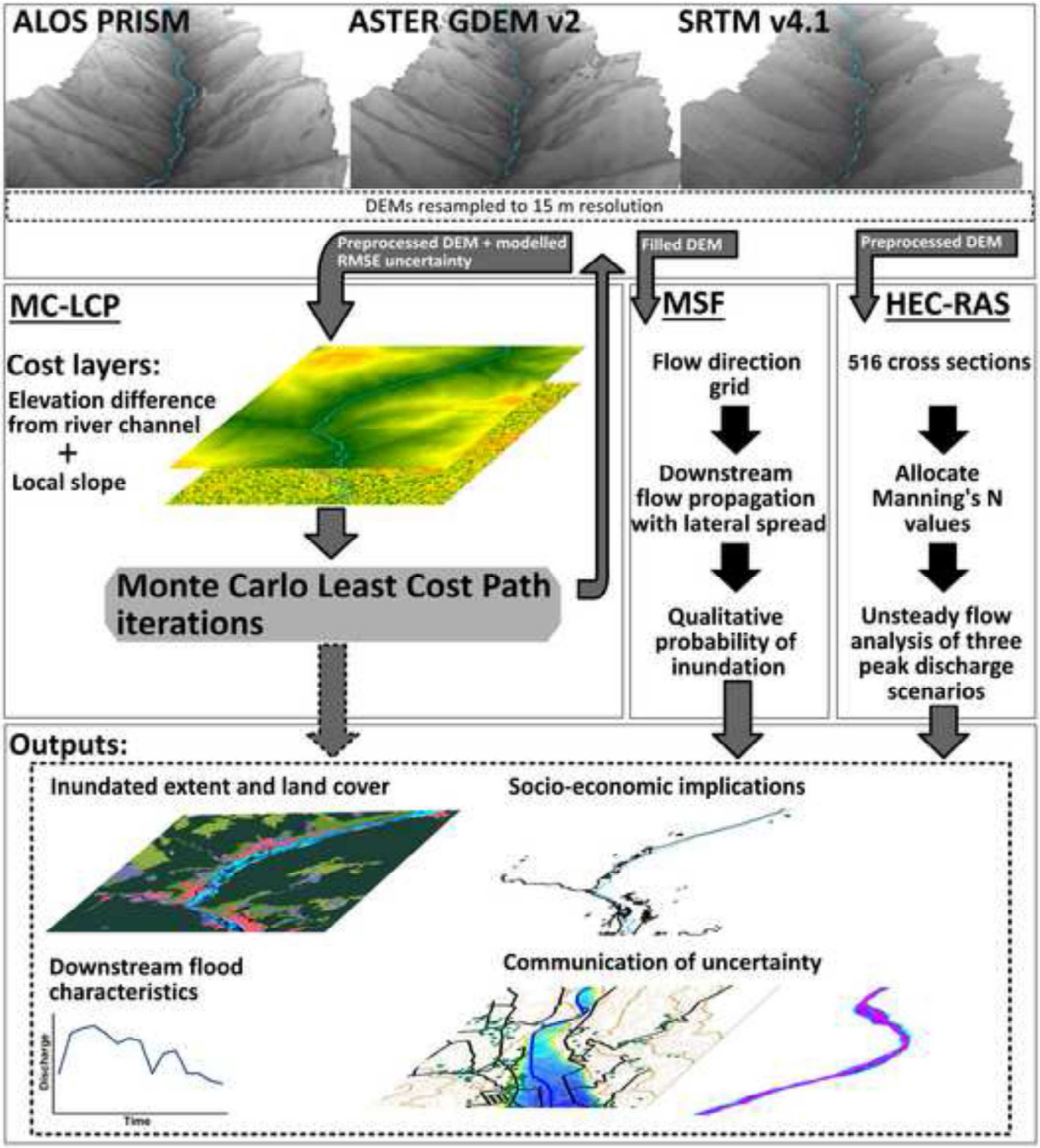

Figure 4

Click here to download high resolution image

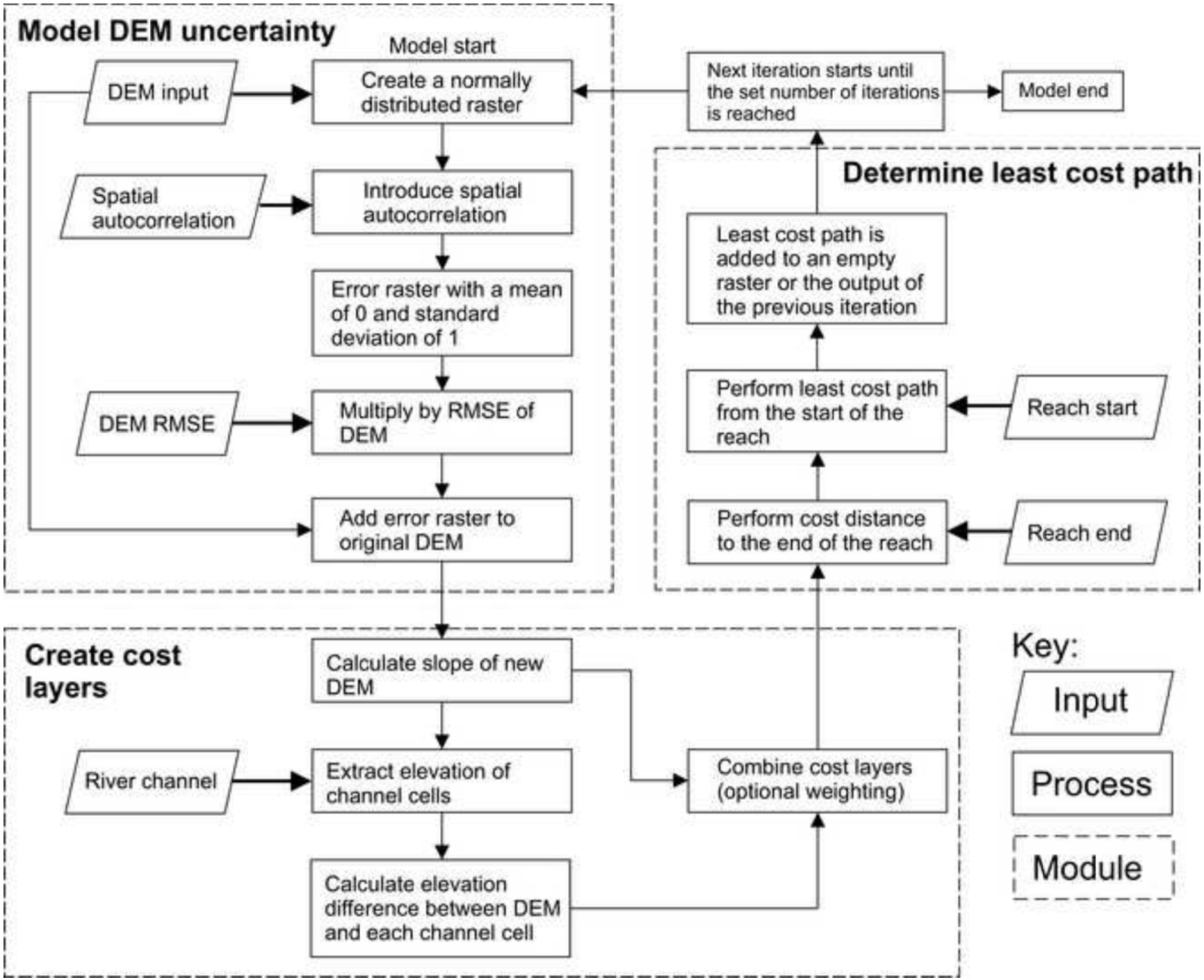

Figure 5
Click here to download high resolution image

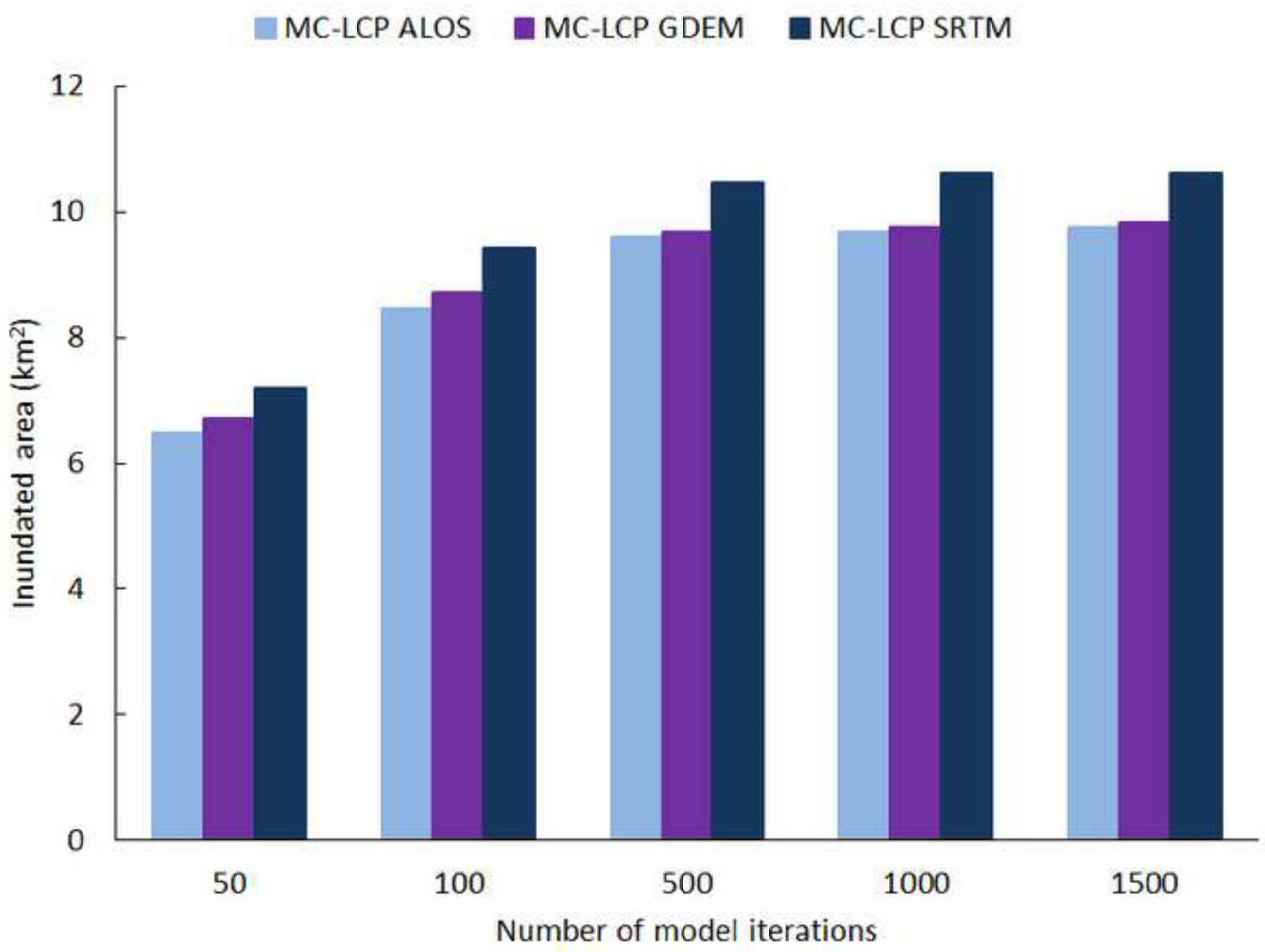

Figure 6
Click here to download high resolution image

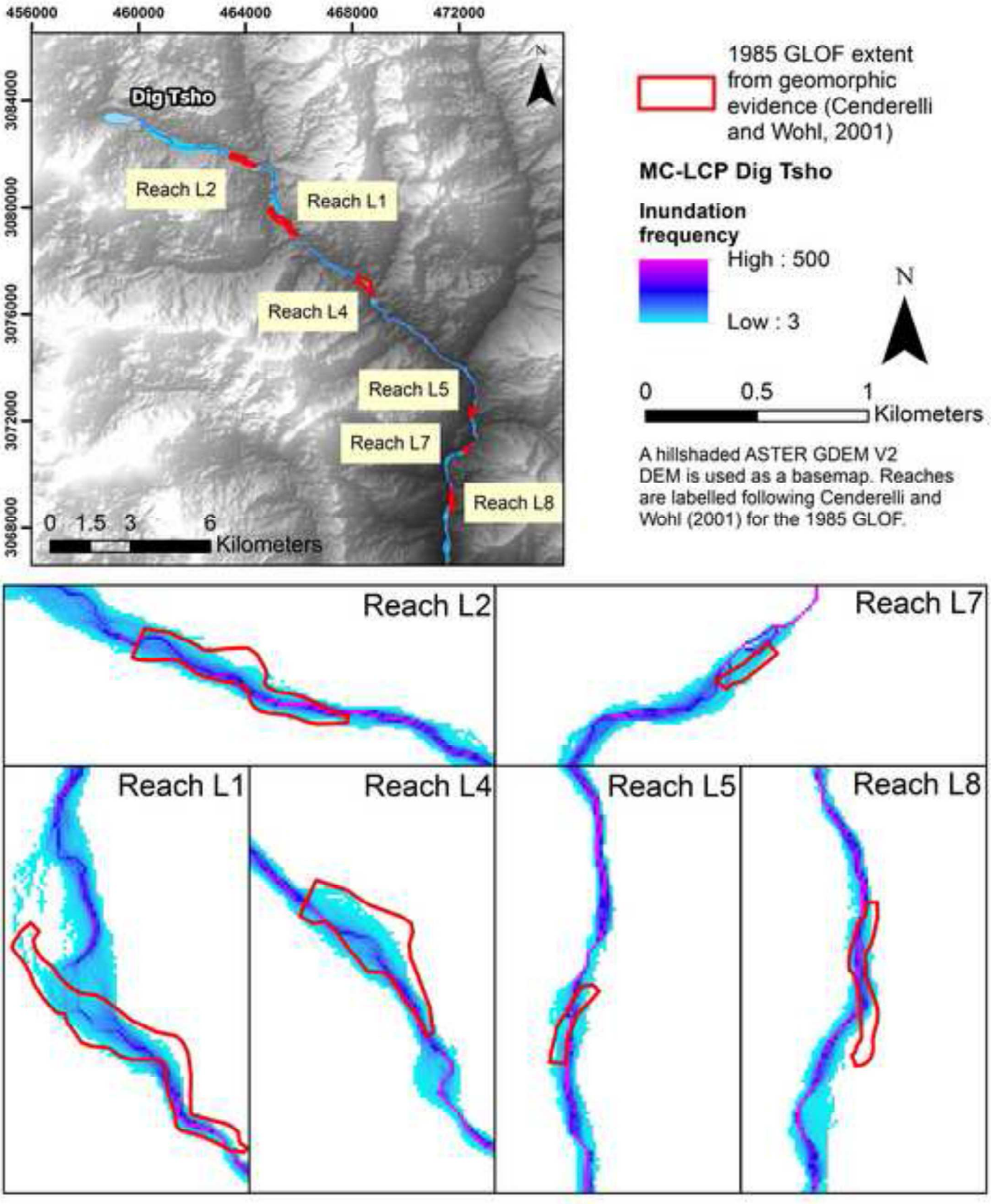

Figure 7
Click here to download high resolution image

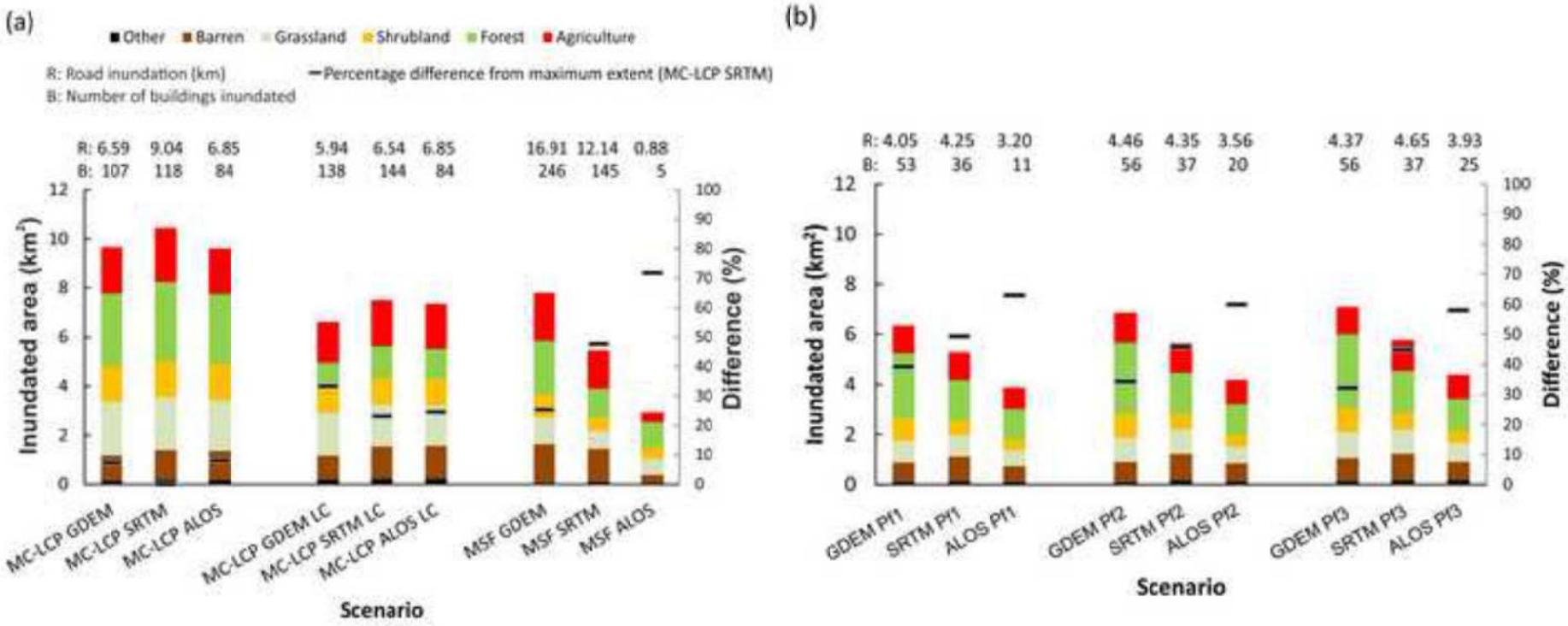

Figure8

Click here to download high resolution image

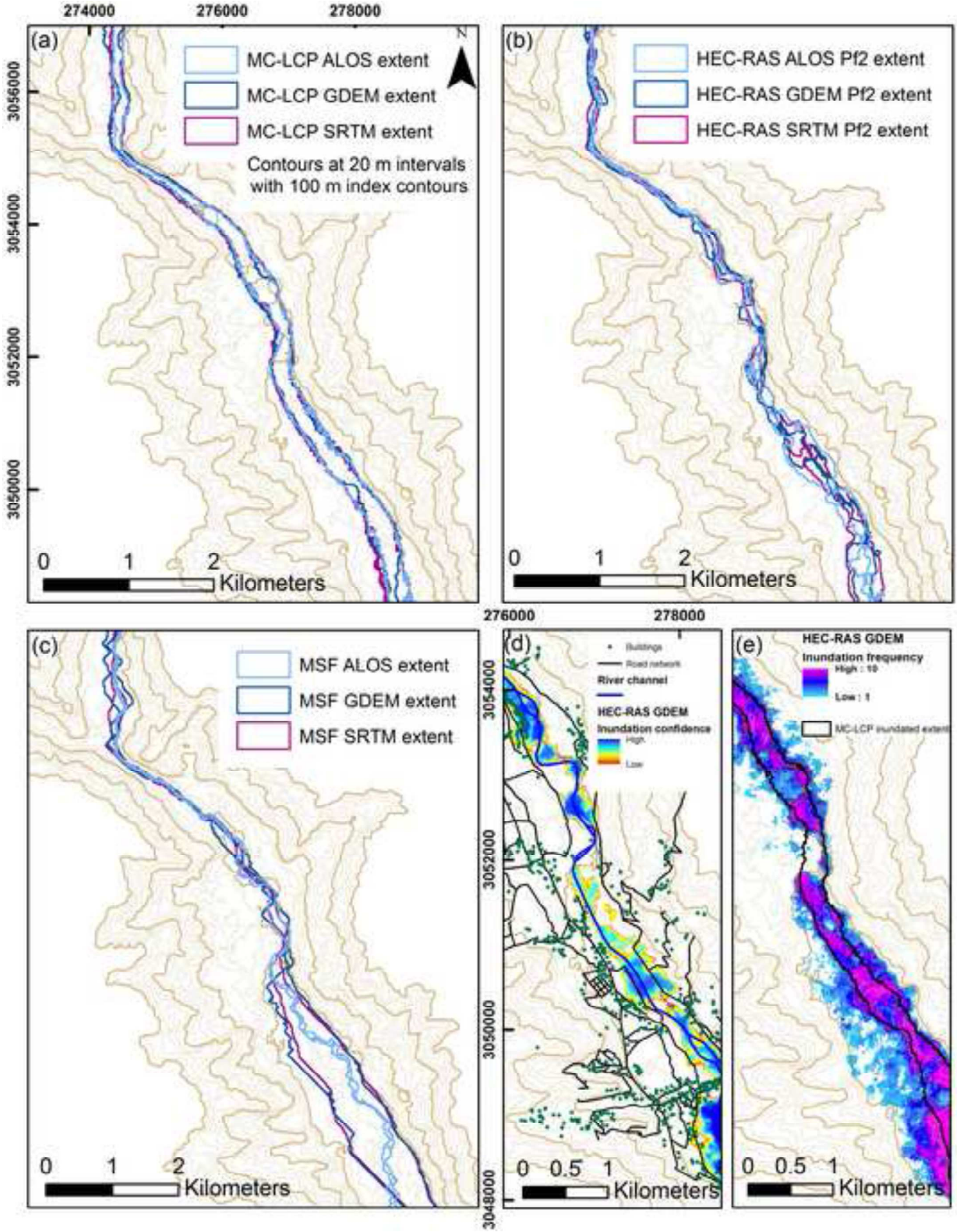

Figure 9

Click here to download high resolution image

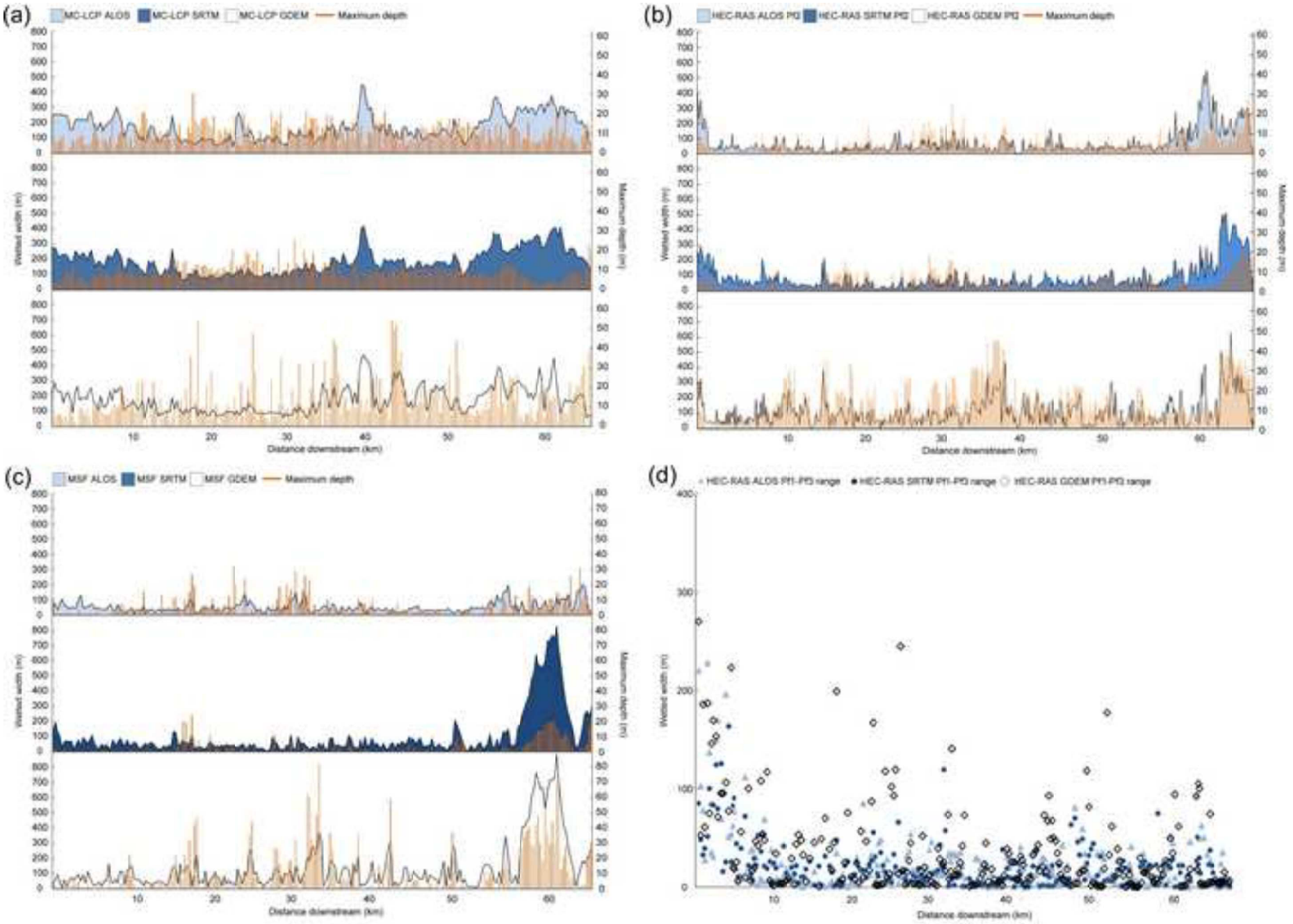

Figure 10

Click here to download high resolution image

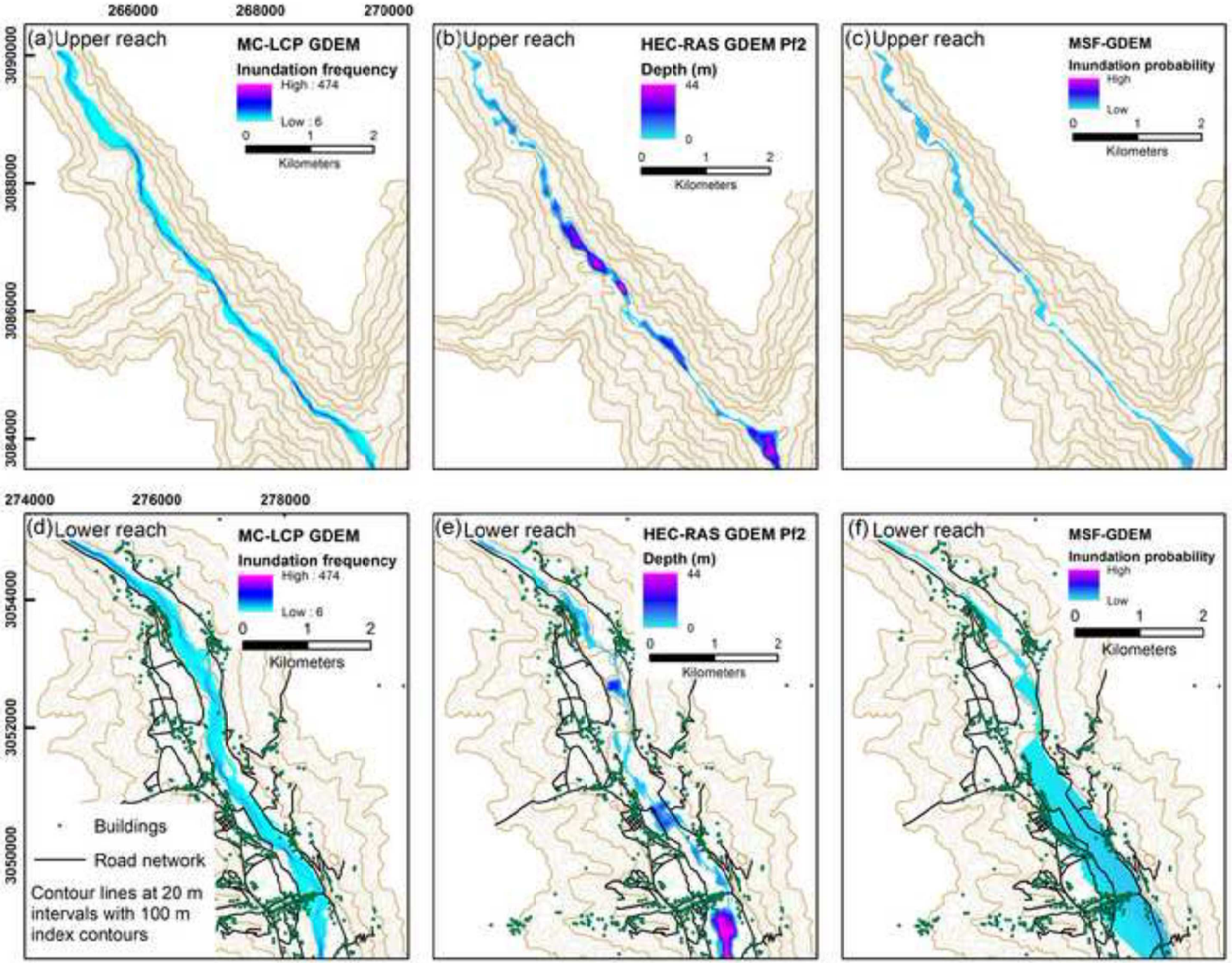

Sup Figure 1

Click here to download high resolution image